Extreme ozone episodes in a major Mediterranean urban area

Jordi Massagué[1,2], Eduardo Torre-Pascual[3], Cristina Carnerero[1,4,*], Miguel Escudero[5], Andrés Alastuey[1], Marco Pandolfi[1], Xavier Querol[1], Gotzon Gangoiti[3]

[1]Institute of Environmental Assessment and Water Research (IDAEA-CSIC), Barcelona, 08034, Spain

[2]Department of Mining, Industrial and ICT Engineering, Universitat Politècnica de Catalunya-BarcelonaTech, (UPC), Manresa, 08242, Spain

[3]Faculty of Engineering Bilbao. University of the Basque Country (UPV/EHU), Bilbao, 48013, Spain

[4]Department of Civil and Environmental Engineering, Universitat Politècnica de Catalunya-BarcelonaTech, (UPC), Barcelona, 08034, Spain

[5]Department of Applied Physics. School of Engineering and Architecture. Universidad de Zaragoza (UNIZAR), Zaragoza, 50018, Spain

*Current affiliation: Barcelona Supercomputing Centre, Barcelona, 08034, Spain

Correspondence to: Jordi Massagué (jordi.massague@idaea.csic.es)

Abstract. This study analyse~~d~~s three extreme ozone (O_3) episodes that occurred in Barcelona (NE Spain) during the summers of 2015, 2018, and 2019. These episodes exceeded the ~~These episodes were the only instances since at least the year 2000 when the~~ EU's hourly information threshold (180 µg·m^{-3}) for the first time since at least 2000, raising~~was exceeded in the city.~~ concerns due to ~~Understanding the phenomenology of these episodes is crucial owing to~~ Barcelona's large population. ~~Using~~ Employing experimental data and ~~diverse~~ various modelling tools, ~~the~~ our main objective wa~~s~~i~~s~~ to elucidate the underlying phenomena of these recent ~~extreme~~ O_3 episodes~~, identify shared patterns~~ and improve ~~future predictions~~predictive capabilities. The ~~results~~findings indicate~~revealed a complex interplay of~~ that the factors contributing to the~~se occurrences~~ ~~episodes~~are largely consistent across episodes.~~,~~ These factors, with estimated O_3 contributions specified for particular instances, comprise: (i) initial O_3 accumulation in surrounding coastal areas, (ii) weekend occurrence, accompanied by the corresponding weekend effect (+15 µg·m^{-3}), and (iii) the prevalence of Tramontana meteorological conditions during above-normal temperatures, which (iv) force the convergence of multiregional polluted air masses to the city (+45–65 µg·m^{-3}). Major source areas include regions of southern France through the Gulf of Lion, the interior of the Mediterranean, and eastern Spanish coastal regions, including Barcelona's pollution plume. ~~including (i) initial regional O_3 accumulation, (ii) the potential impact of Tramontana winds on O_3 transport into the western Mediterranean basin, (iii) O_3 accumulation via vertical recirculation and horizontal circulation of the local pollution plume in a weakened sea breeze regime, (iv) convergence of polluted air masses from multiple sources, (v) calm upper layer winds, (vi) the weekend effect, and (vii) abnormally high temperatures.~~ Some of these factors, which may manifest in the days preceding the episodes, are ~~readily~~ observable or can be anticipated. ~~Consequently, the findings of this~~This study enhances ~~the~~ understanding of the mechanisms driving ~~these~~ extreme O_3 episodes recently observed in Barcelona and provides ~~their~~ prediction.

1. Introduction

35 Tropospheric ozone (O$_3$) is a strong oxidising secondary atmospheric pollutant, adversely affecting human health, ecosystems and materials (WHO, ~~2006,~~ 2013a, b, 2021; GBD, 2016; Fowler et al., 2009; IPCC, 2021). ~~Its~~ The formation of O$_3$ depends primarily on complex photochemical reactions between precursors (mainly nitrogen oxides (NOx), ~~CH$_4$, CO~~ and non-methane volatile organic compounds (VOCs)), ~~and solar radiation~~ in the presence of sunlight. The NOx/VOC ratio considerably influences O$_3$ formation. Urban areas, with high NOx levels, typically experience VOC-limited O$_3$ production (Sillman et al., 1999; Sillman and He, 2002), leading

40 to the 'weekend effect'—higher O$_3$ concentrations on non-working days predominantly due to reduced emissions of O$_3$-depleting pollutants (Heuss et al., 2003; Jiménez et al., 2005). Conversely, suburban and rural environments, with low NOx/VOC levels, typically exhibit NOx-limited O$_3$ formation. ~~Its~~ The production of O$_3$ is enhanced by high solar radiation and ~~high~~ temperatures, and low relative humidity (Monks et al., 2015), contributing to extreme O$_3$ events. These events have been linked to heat waves and increased mortality globally (e.g., Vautard et al., 2007; Guo et al., 2017; Pu et al., 2017; Jaen et al., 2021).

45 ~~The NOx/VOC ratio considerably influences O$_3$ formation. O$_3$ production is typically VOC-limited in urban environments owing to relatively high NOx levels, while it is typically NOx-limited in suburban and rural environments where NOx/VOC levels are low (Sillman et al., 1999; Sillman and He, 2002). In urban environments, the VOC-limited regime typically results in the "weekend effect", where O$_3$ concentrations are typically higher on non-working days. This is due to lower emissions of O$_3$-depleting pollutants (Heuss et al., 2003; Jiménez et al., 2005).~~

50 Concentrations of O$_3$ in Barcelona (NE Spain) are not particularly higher than in other regions of the country (Querol et al., 2016; Massagué et al., 2023) likely owing to strong O$_3$ titration and ozonolysis (Monks et al., 2015) ~~caused by local emissions of NO and VOCs~~, resulting in infrequent exceedances of the legal thresholds set by the European AQ Directive (2008/50/EC; EC, 2008). However, ~~since at least 2000,~~ exceedances of the hourly Information Threshold (IT, O$_3$ concentration >180 µg·m^{-3}) ~~have only been~~ were detected in 2015, 2018 and 2019 (Gencat, 2022), representing the only instances of such occurrences since

55 at least the year 2000.~~.~~ These ~~extreme~~ events exposed a large population segment to exceptionally high O$_3$ concentrations, which is particularly concerning as Barcelona is Spain's second most populous urban area.~~, with the highest population density neighbourhoods in Europe (Batista et al., 2021).~~

This study aims to identify the underlying factors contributing to recent episodes of extreme O$_3$ concentrations in Barcelona by investigating the meteorological, transport, and formation mechanisms associated to these occurrences. Additionally, it

60 aims to gain novel insights to advance future event prediction. ~~This study aimed to elucidate the underlying phenomena behind the recent episodes of extreme O$_3$ concentrations in Barcelona, determine potential common patterns and obtain relevant information to enhance the prediction of future occurrences.~~ The study is structured as follows: Section 2 outlines the methodology, while Section 3 (Results and Discussion) is subdivided into three parts (3.2, 3.3, and 3.4), where each episode is systematically analysed, adhering to the same order: discussion of the meteorological context, surface observations, and

65 trajectory and photochemical simulations. The final section presents a joint analysis of the episodes, including estimations of O_3 contributions and drawing conclusions from the combined findings.

2. Methodology

To comprehensively analyse the episodes, we propose a combined methodology that integrates multiple approaches and datasets, including ground-based and satellite observational data, meteorological ~~reanalysis~~reanalyses, high-resolution
70 backward and forward trajectory simulations and photochemical ~~simulations~~modelling.

2.1 Study area

This study is focused on Barcelona, Spain's second most populous municipality, located on the NE coast of the Iberian Peninsula (IP), with 1.6 million inhabitants within the city limits and up to 5.2 million in neighbouring urban areas (MITMA, 2021).

75 Barcelona and its surrounding metropolitan area (BMA) are significant sources of NOx and VOC emissions from road traffic, industry, shipping activities and domestic sources. In summer, air masses loaded with O_3 and its precursors are transported inland and, combined with high biogenic VOC emissions from nearby forested areas, may cause severe O_3 episodes in downwind areas (e.g. Toll and Balsano, 2000; Pérez et al., 2004; Gonçalves et al., 2009; Diéguez et al., 2009; Valverde et al., 2016; Querol et al., 2017).

80 Similar to the BMA, emissions of industrial and urban pollutants from Tarragona contribute to the typical high O_3 levels in the northern and northwestern areas (Querol et al., 2016). Tarragona is located on the coast 90 km SW of Barcelona (Fig 1b), and it is surrounded by notable chemical and petrochemical industrial complexes.
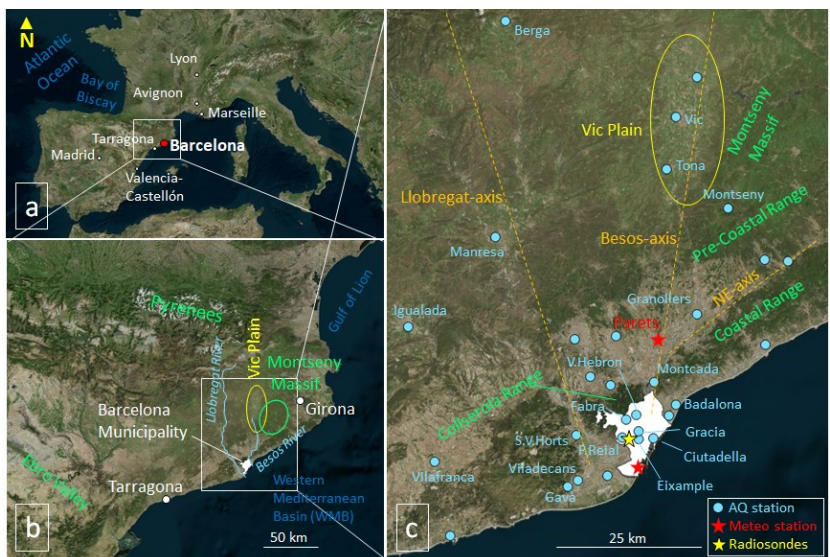
Localisation	Name of AQMS	Type	European code	Latitude (deg.)	Longitude (deg.)	Altitude (m ~~above sea level~~ASL)
Barcelona	*Port*	*Meteo*	*D5*	*41.31725*	*2.16537*	*3*
	Faculty of Physics Univ. Bcn	*Radiosondes*	*-*	*41.38553*	*2.11720*	*70*
	Ciutadella	UB	ES1679A	41.38641	2.18742	7
	Fabra	SB	ES2090A	41.41840	2.12390	418
	P.Reial	UB	ES1992A	41.38748	2.11515	81
	Gràcia	UT	ES1480A	41.39874	2.15339	57
	V.Hebron	UB	ES1856A	41.42608	2.14799	136
	Eixample	UT	ES1438A	41.38534	2.15382	26
Barcelona Metropolitan Area (BMA)	Badalona	UB	ES1892A	41.44398	2.23788	7
	Gava	SB	ES1910A	41.30311	1.99152	25
	Viladecans	SB	ES1903A	41.31348	2.01382	14
	S.V Horts	SB	ES0694A	41.39216	2.00980	38
	Montcada	ST	ES0584A	41.48202	2.18830	34
	Granollers	UT	ES1891A	41.59867	2.28712	133
	Parets	*Meteo*	*XG*	*41.56734*	*2.22619*	*123*
Montseny Massif	Montseny	RB	ES1778A	41.77934	2.35802	693
Vic Plain	Tona	RB	ES1923A	41.84603	2.21758	620
	Vic	SB	ES1642A	41.93567	2.23857	498

Figure 1. Top: Area of study. Blue dots represent air quality monitoring stations (AQMSs). Only names of AQMSs used in the study are displayed in (c); others are kept for reference. Red stars indicate meteorological stations. The yellow star indicates the location of radiosounding launches. Bottom: Main characteristics of the AQMSs. Types are UB−urban background, UT−urban traffic, SB−suburban background, ST−suburban traffic and RB−rural background. Meteorological stations are identified with their

meteorological office's code. For Barcelona, wind data are from the Barcelona port, and temperature and relative humidity data are from the same location as the AQMS Fabra. The white-shaded area depicts the municipality of Barcelona.

Gangoiti et al. (2001, 2006) described the recurrent warm-season weather pattern in the region, directing Mistral and Tramontana (NW and N through the Gulf of Lion) winds into the lower layers of the WMB through the Gulf of Lion. This flow has a diurnal pulsation, shifting eastward during the daytime and southward in the late evening and night due to general compensatory subsidence coinciding with sea breezes. Consequently, air masses entering through the Gulf of Lion at night can be captured by sea breezes along the eastern coast of Iberia, re-entering in the same cycles over several days.

In this context, accumulation by the vertical recirculation of air masses loaded with O_3 may occur over several days, particularly during the typical summer absence of significant synoptic advections. Therefore, under persistent anticyclonic conditions, air masses can gradually accumulate O_3, leading to progressively higher concentrations in the same areas on subsequent days. These situations typically end with the arrival of a frontal system, which vents out the accumulated O_3 and can eventually transport prefrontal dust-loaded African air masses with different properties leading the cold front (Millán et al., 1997, 2000, 2002; Toll and Baldasano, 2000; Gangoiti et al., 2001; ~~Pérez et al., 2004;~~ Gangoiti et al., 2006; Jiménez et al., 2005; Diéguez at al., 2009, 2014; Millán, 2014; Querol et al., 2017).

In the study area, these conditions can lead to either an open or closed circulation system (Querol et al., 2017 and references therein). Thus, the BMA can ~~act~~ function as a significant source of O_3 precursors, ~~while~~ with downwind areas ~~act~~ serving as receptor zones. Hence, we examined the evolution of surface O_3 concentrations ~~of surface O_3~~ not only at AQMSs within the city where the episodes were recorded but also at locations along the mentioned axes and surroundings (Fig. 1c).

2.2 Observational data

We employed the following datasets:

-Hourly O_3, NO_2 and NO concentrations provided by the European Environment Agency (EEA, https://www.eea.europa.eu/data-and-maps/data/aqereporting-9) for all the AQMSs with available O_3 measurements during the study periods in southern France and NE Spain;

-Hourly meteorological data (temperature, relative humidity, solar radiation and wind speed/direction) from two meteorological stations located in the study area (Fig. 1) retrieved from the Meteorological Office of Catalonia (https://analisi.transparenciacatalunya.cat/en/Medi-Ambient/Dades-meteorol-giques-de-la-XEMA/nzvn-apee);

-High-resolution vertical meteorological data (temperature, relative humidity and wind speed/direction) from radiosoundings conducted in Barcelona at 00 and 12 UTC provided by the Faculty of Physics, University of Barcelona. We also used estimations of the mixing layer height (MLH) at 12 UTC using the simple parcel method (Holzworth et al., 1964); ~~and~~

-Daily NO_2 tropospheric column observations (only for the 2019 episode) obtained from TROPOMI, a high-resolution nadir-viewing satellite sensor aboard the ESA's Sentinel-5 Precursor (Veefkind et al., 2012). Observations at 13:30 local solar time organised as daily gridded data (5.5×3.5 km^2 resolution) were derived from the offline operational product (Van Geffen et al., 2019) using a script in Google Earth Engine (Gorelick et al., 2017) and a quality assurance of >0.75.

2.3 Modelling tools

We conducted high-resolution backward and forward trajectory simulations using the mesoscale Regional Atmospheric Modelling System (RAMS) (http://www.atmet.com/software/rams_soft.shtml) and the HYbrid PArticle Concentration and Transport (HYPACT) model (http://www.atmet.com/software/hypact_soft.shtml). We used three nested square domains, centred in on Barcelona, with grid resolutions of 3, 12 and 48 km, extending up to 190, 1000 and 2600 km around the city, respectively. Backward trajectories ending at less than 400 m above ground level (AGL) in the city were used to identify upwind sources of precursors and O_3. Tracer particles emitted from a selection of these upwind sources (cities) were then used to evaluate the eventual convergence of forward trajectories into Barcelona, using a similar methodology as in Gangoiti et al. (2001, 2002, 2006, 2011), and more recently I in't Veld et al. (2021). Because we used constant emission rates from all the city sources, this tool could not evaluate the real contribution of each source but the efficiency of the atmospheric transport into the planetary boundary layer (PBL) of Barcelona. This was conducted at an hourly resolution during the pollution episode. The methodology is useful for identifying possible location of sources and the potential of convergence from different source regions. The PBL height and ground elevation influence the amount of particles reaching the receptor sites and the distribution of confluent sources. Receptor sites considered in Barcelona were Ciutadella and Palau Reial, located at nearly sea level, as well as Fabra, located 400 m etres above sea level ASL. These locations align with the corresponding AQMSs with the same names (Fig. 1).

The PBL height was retrieved from the ERA5 reanalysis from the European Centre for Medium-range Weather Forecasts (ECMWF), https://cds.climate.copernicus.eu/cdsapp#!/dataset/reanalysis-era5-single-levels?tab=form. Data used were hourly ERA5 reanalysis at midday in the nearest grid point to the corresponding coordinates of the Palau Reial AQMS.

We also conducted photochemistry and dispersion simulations using the Comprehensive Air Quality Model with extensions (CAMx, version 6.5, Ramboll Environment and Health, 2018). We employed the gas-phase mechanism CB6r4 and used the SPECIATE tool (EPA, 2016) to speciate NOx and VOCs. For a detailed description of the model, see Torre-Pascual et al. (2023), which analysed a 2018 high O_3 episode in the Bay of Biscay a few days prior to the 2018 Barcelona episode assessed here. In our study, we used the same general model configurations described in the reference but with higher vertical resolution, 44 levels up to 6000 m AGL, as shown in Section S5 4. Emissions were simulated using MEGAN 3.0 to account for biogenic emissions and EDGAR v4.3.2 for anthropogenic emissions. The MEGAN model incorporated recently updated Spanish land

use and vegetation map databases sourced from the National Forest Inventory, as demonstrated in Torre-Pascual et al., (2021). We utilised version 4.3.2 of the Emission Database for Global Atmospheric Research (EDGAR) global anthropogenic emission inventory (Crippa et al., 2018), published in December 2017. This inventory includes anthropogenic emissions from the European and African continents within our study area. We focused on analysing the following key compounds for tropospheric O_3 pollution episodes: CO, NH_3, VOCs, NOx, SO_2 and CH_4. Emissions change significantly over time, but due to ease of calculation, and to conduct an analysis independent of emission variations, we have utilised the emissions inventory published in the year 2017, valid for monthly averages for 2010. The use of this inventory will introduce uncertainties but may not impact the main qualitative findings of our study.

The results of photochemical models in air pollution studies typically present pollutant concentrations and wind fields at the surface level. To enhance the visualisation and interpretation of the dynamics driving O_3 episodes, Torre-Pascual et al. (2023) recommended expanding the analyses to higher atmospheric levels, particularly in complex terrains, such as the Spanish territory, due to the multiple processes involved. In this study, we present the results of integrated O_3 concentrations and average wind fields at up to 500 m AGL, surface and upper-level O_3 concentrations and wind fields, and vertical cross sections along the Besòs-axis to illustrate recirculations, fumigations and subsidence processes. Section S6 (supplemental) contains a brief assessment of the simulations performance conducted by the photochemical model.

3. Results and discussion

3.1 Extreme episodes in Barcelona

Table 1 summarises the only three episodes when Europe's IT has been exceeded in Barcelona since (at least) 2000. Notably, during the 2019 episode, concentrations approached Europe's hourly alert threshold (AT, O_3 concentration >240 µg·m^{-3}).

Table 1. General information about the episodes with Europe's Information Threshold (IT) exceedances. Types of air quality monitoring stations (AQMSs) include UB−urban background, SB−suburban background and UT−urban traffic.

Date of IT exceedance (dd/mm/yyyy)	Day of the week	Start time (h UTC)	Number of hours above the IT	Name of AQMS (Type)	O_3 1h max. concentration (µg·m^{-3})	Declared heatwave
06/06/2015	Saturday	13	1	Ciutadella (UB)	206	no
04/08/2018	Saturday	14	1	Fabra (SB)	190	yes
		16	3	Fabra (SB)	197	
		16	2	Gràcia (UT)	197	
		18	1	V. Hebron (UB)	187	
05/08/2018	Sunday	13	2	Ciutadella (UB)	190	
		15	1	Fabra (SB)	182	
29/06/2019	Saturday	14	2	Ciutadella (UB)	190	yes
		14	2	Eixample (UT)	211	
		14	9	Fabra (SB)	236	

		15	1	P. Reial (UB)	229	
		16	1	V. Hebron (UB)	196	
		18	1	V. Hebron (UB)	184	

~~Below, we present a detailed analysis of the three episodes individually (subsections 3.2, 3.3 and 3.4). Within each subsection, we present and discuss results related to the meteorological context, observations and simulations. Annexes are included for each episode (Sections S1 to S3 in the supplemental information) to organise the extensive supplementary material.~~

3.2 2015 episode (6 June)

3.2.1 Meteorological context

Synoptic situation

From 1 to 5 June 2015, a low-pressure system was located NW of the British Isles (observed from 3 June in Fig. 2), while a high-pressure ridge moved from SW to NE across the IP towards central Europe. This situation favoured persistent E winds in the WMB, which turned southeast along the Catalan coast and then south with sea breezes. The ERA-INTERIM reanalysis indicated a 50 ppb (~100 $\mu g \cdot m^{-3}$) O_3 accumulation at low levels (1000–925 hPa) over the Catalan coast, possibly due to the mentioned persistent E winds from various origins, including Italy and the Balearic Islands. In this scenario, the usual diurnal Tramontana cycle (Gangoiti et al., 2001) was absent, and in the interior of the IP, there might have been the uncoupling of nocturnal drainage flows with valley-down or seaward winds and diurnal couplings with the combined flows of coastal breezes and synoptic E winds.

On 6 June, there was a change in surface pressures in the Bay of Biscay and southern France, with higher pressures than in the Mediterranean (Fig. 2). As a result, Tramontana (N) winds developed and persisted until 9 June, at which time there was a change in the synoptic conditions (not shown).

Local observations

Notably, the maximum temperatures (Fig. S1.2b~~d~~) during this episode in the Barcelona area were 3–4°C higher than the usual June temperatures (Observatori Fabra, 2022), despite it not being a declared heatwave as with the other episodes.

The radiosoundings conducted in Barcelona (Fig. S1.1) showed persistent E winds above 1500–2000 m ASL throughout the period, while land–sea breezes and Tramontana cycles dominated in the lower layers. Before 6 June, lower atmosphere winds followed a daily pattern of W–SW at night, shifting to the S during the day (Fig. S1.1), resulting in a net inland transport towards the N due to coastal sea breeze regimes. The change in synoptic conditions on 6 June caused a noticeable change in the lower atmosphere winds, with an abrupt shift to the E in the early morning. This was accompanied by a temperature increase and relative humidity decrease (Fig. S1.2a–b), likely related to a brief period of vertical coupling with dry easterlies

from the free atmosphere (Fig. S1.1). Then, a progressive increase in humidity, coinciding with the wind backing to the S ~~(Fig. S1.2b)~~, marked the onset of the sea breeze. Subsequently, a surface temperature inversion developed at 200 m during the following night, leading to calm conditions in a saturated air layer completely decoupled from the easterlies above.

200
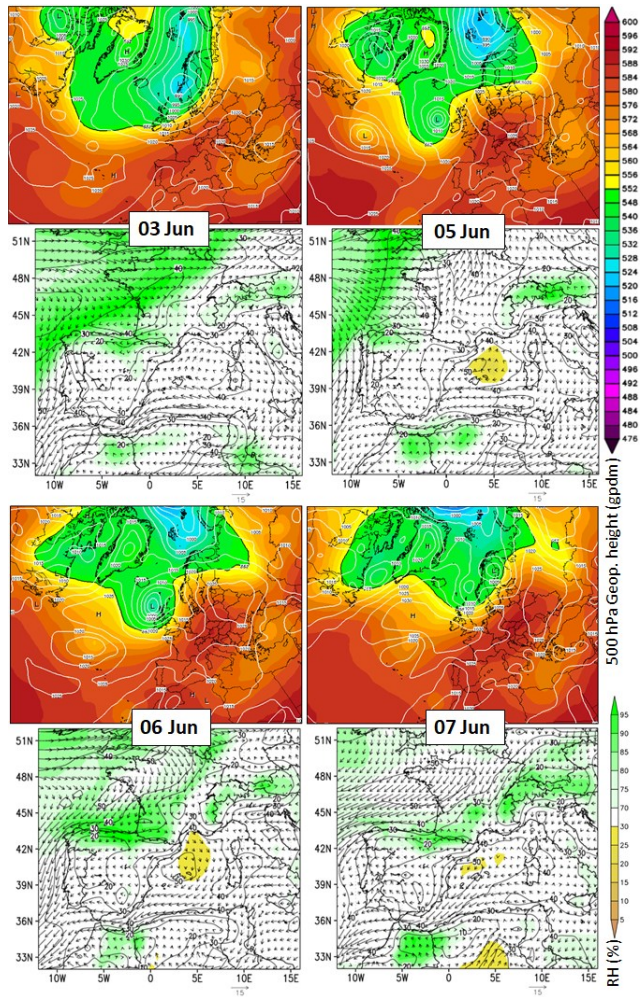
Figure 2. Episode 2015. For each day, (top) Climate Forecast System Reanalysis for the 500 hPa geopotential heights and mean sea level pressure (hPa) at 00 UTC (source: www.wetterzentrale.de), (bottom) ERA-INTERIM (ECMWF) reanalysis (0.75° resolution) of O$_3$ concentration (ppb, contour-lines; 1 ppb ≈ 2 μg·m^{-3} at sea level), and relative humidity (shaded colours) and wind field on the 1000–925 hPa level.

205

3.2.2 Surface O_3 concentrations

From 3 to 5 June, diurnal O_3 concentrations in the BMA (Fig. 3) were relatively low to moderate (up to 60–113 $\mu g \cdot m^{-3}$),
210 displaying a nearly square-shaped daily cycle observed in low-altitude coastal locations in the WMB (e.g. Millan et al., 2000).
This pattern showed peak concentrations during the central diurnal hours and the lowest levels at night (Fig. 3b–c). Traffic
stations (Eixample, Montcada or Granollers) had minimal concentrations due to O_3 titration from local emissions (e.g., Solberg
et al., 2005). On 4 and 5 June, the aforementioned persistent moderate S winds in the lower 1000 m of the atmosphere led to
significantly high O_3 concentrations downwind of the BMA. This was evident in AQMSs, such as Berga (at the end of the
215 Llobregat-axis) and stations in the Vic Plain (at the end of the Besòs-axis), where the IT was either exceeded or nearly reached
(Fig. 3a and c).

The O_3 daily cycles along the Besòs-axis (Fig. 3c) and the aforementioned combined upslope winds and sea breezes suggest
the usual dynamics of summer O_3 episodes downwind (northward) of Barcelona (e.g., Querol et al., 2017) in the days before
the episode. This recurring pattern, termed here "Besòs-axis dynamics", is characterised by the gradual increase in diurnal O_3
220 concentrations from Barcelona to the Vic Plain (see the O_3 gradients highlighted in Fig. 3c) and the early-afternoon O_3 peaks
that occur at later times based on their distance from Barcelona, illustrating the northwards path of the BMA plume loaded
with new O_3 contributions.

The rural background station in Montseny (~700 m ASL) showed minimal daily O_3 variation, with concentrations remaining
constant at approximately 120 $\mu g \cdot m^{-3}$ (Fig. 3c). This is due to the limited nighttime consumption, owing to its remote location
225 away from O_3-consuming emissions and above the stable nocturnal boundary layer, ensuring a continuous supply of O_3 from
reservoir layers (e.g., Millán et al., 2000; Millán et al., 2002; Chevalier et al., 2007). A detailed discussion of multiple typified
O_3 cycles in an air basin, with similar O_3 phenomenology to our study area, can be found in Millán et al. (2000).

On Saturday, 6 June (episode in Barcelona), only one station exceeded the IT, but most sites in the city, including the traffic
type, recorded very high O_3 concentrations (up to 179 $\mu g \cdot m^{-3}$) and a considerable concentration peak at 12–13 UTC (Fig. 3b).
230 This coincided with the shift in surface winds from the NE to SE during the afternoon (Fig .S1.2a). Stations along the Besòs-
axis, farther from Barcelona, recorded significantly lower diurnal O_3 concentrations compared to the preceding days (<140
$\mu g \cdot m^{-3}$), with constant levels in the Vic Plain, lacking the usual early-afternoon O_3 peak (Fig. 3c). The development of a
weaker breeze, as mentioned earlier, along with reduced weekend emissions of precursors from the BMA (see NOx
concentrations in Fig. S1.3), likely contributed to this pattern. This behaviour is common during summer weekends, with the
235 Vic Plain typically exhibiting lower O_3 levels than on weekdays (e.g., Massagué et al., 2019).
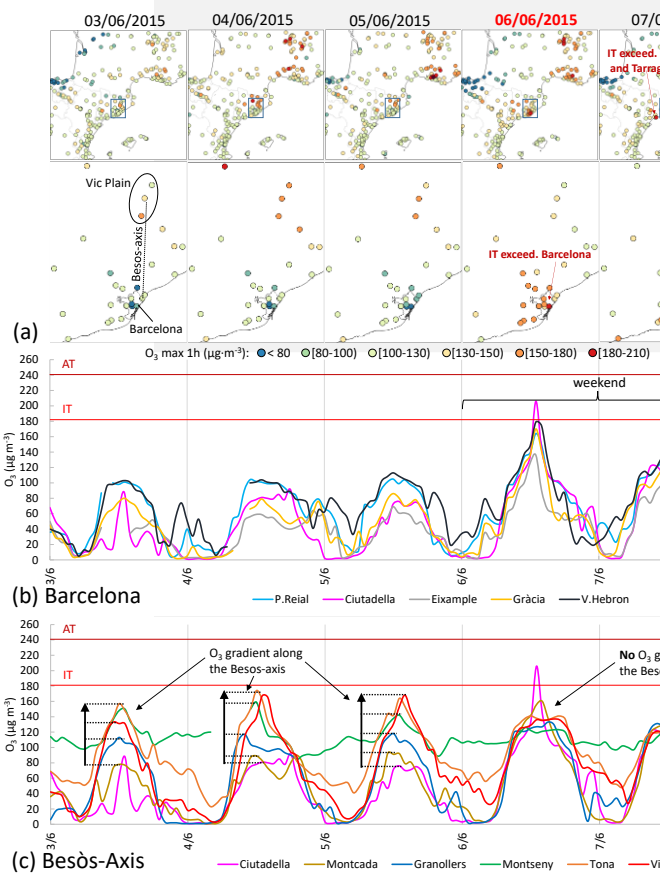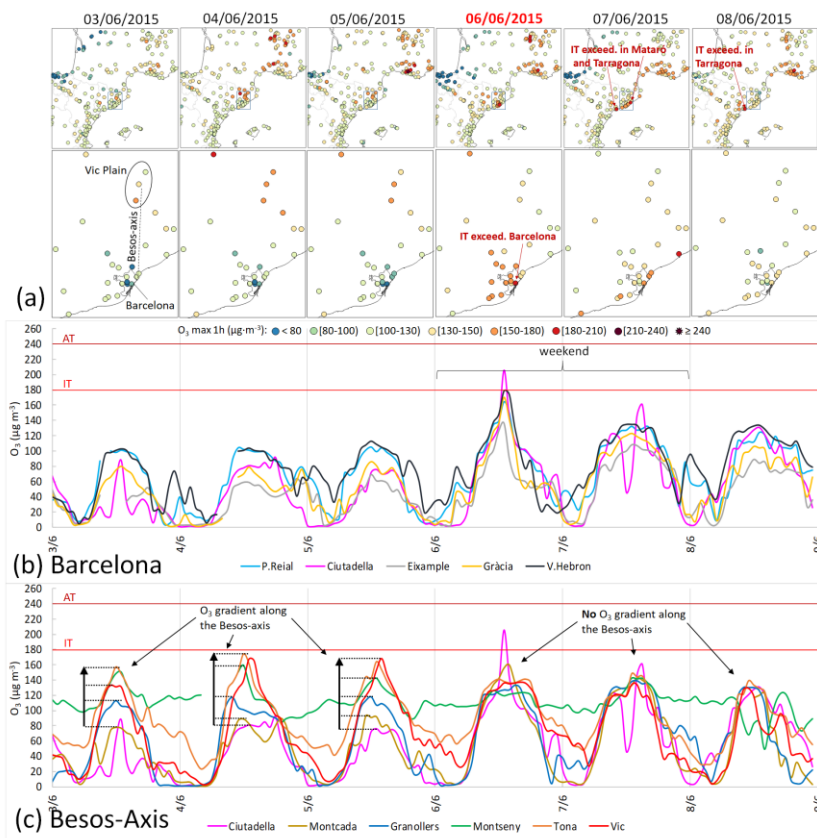
Figure 3. Episode 2015. (a) Spatial distribution of maximum hourly O₃ concentrations. Daily O₃ cycles at the surface stations: (b) Barcelona city (no data from Fabra), (c) along the Besòs-axis, ordered with increasing distance to Barcelona: Ciutadella, Montcada, Granollers, Montseny, Tona and Vic. Horizontal red lines represent Information and Alert Thresholds of the EU's Directive (IT and AT).

In the subsequent days, peak O₃ concentrations in the city decreased but remained significantly higher than before the episode (Fig. 3c), possibly due to the aforementioned O₃ vertical recirculations and the stagnation of air masses over the Barcelona area. This situation contributed to the exceedances of the IT at two relatively close coastal stations on 7 and 8 June (Fig. 3a).

245 By 9 June, O_3 concentrations in the city returned to pre-episode levels (not shown) because of the aforementioned changing meteorological conditions.

3.2.3 Modelling output

Trajectory analyses results

The RAMS/HYPACT analyses (Fig. S1.4) show two groups of arrival trajectories to Barcelona (Ciutadella). First, trajectories

250 on 6 June crossed the WMB with E–SE winds from 3 to 5 June, arriving in Barcelona from the E and S, following the Mediterranean gyre (Fig. S1.4a–e). Second, on 7 June, trajectories passed through southern France from 5 and 6 June with W winds, and then transitioned through the Gulf of Lion with the Tramontana winds (Fig. S1.4c–e).

The temporal evolution of tracer particles (Fig. 4a), emitted in forward trajectories from 18 cities (coloured dots in Fig. 4b) reaching Barcelona's PBL, indicates the highest impacts originated from multiple sources, including Marseille, Toulouse,

255 Tarragona, Palma (de Mallorca), Cagliari, Montpellier, and Barcelona. This was different from the previous days, where the origin was solely Mediterranean: from the E (Palma, Cagliari) and S (Tarragona).
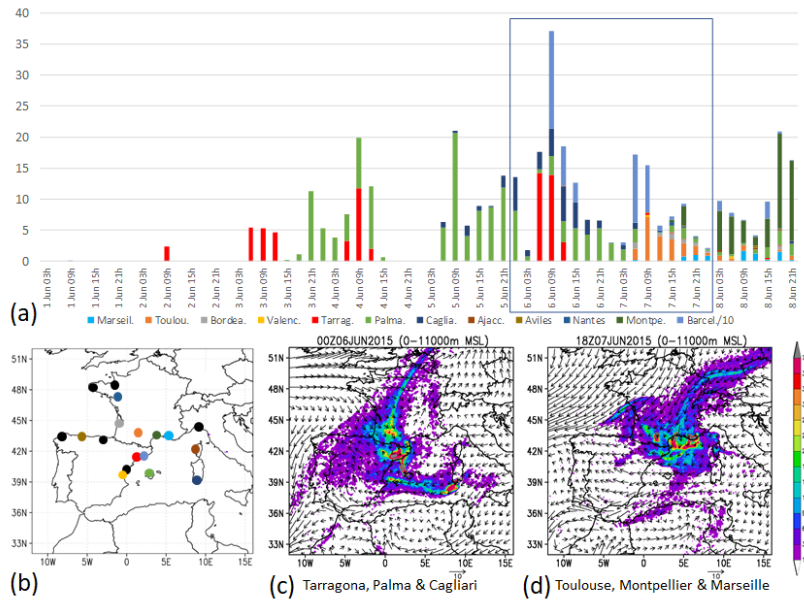
Figure 4. Episode 2015. (a) Temporal evolution of impacts (number of tracer particles) emitted from cities shown in the map (b) and reaching Barcelona PBL (Ciutadella) in forward trajectories. Emission point "Barcelona" impacts were divided by 10 due to proximity to the receptor site. Cities not represented in (a) have a negligible contribution, shown as black dots on the map. Sources in (a) use the same colour code as in (b) map. (c–d) Burden of tracer particles (0–11,000 m) impacting Barcelona during the weekend from three selected Mediterranean cities with the main impact on 6 June (c) from the E and S, and (d) three more sources in southern France with the main impact on 7 June from the N.

Figure S1.5 depicts a Barcelona-originating plume dispersion simulation with northward transport before 6 June and no circulation of coastal emissions over the WMB. Starting on 6 June with Tramontana winds, a land–sea recirculation developed along the Barcelona coast. The plume underwent a complete rotation, with Barcelona at the centre of a convergence zone. Barcelona received pollution from the Gulf of Lion and from the E and SE areas, transported by sea breezes and the Mediterranean gyre. These inputs merged with the local emissions from the E Spanish coast.

The key finding of these analyses is the convergence of a set of multiple sources on the day of the episode, located to the NW of the city (S France), to the E (other Mediterranean cities), to the S (Tarragona) and in Barcelona.

Photochemical model results

Outcomes from the photochemical simulation from 5 June are shown in Figs. 5 and S1.6. The model replicates intense sea breezes along the Catalan coast, aligning with local observations. These breezes transported the BMA plume northeastward, reaching nearly the Pyrenees (Fig. S1.6). The vertical section in the same figure also shows O_3 accumulation northward of the Pyrenees (circle on 5 June at 16 UTC in Fig. S1.6). The presence of a high pressure over the Balearic Islands suggests subsidence of upper layers over the sea. In the afternoon, stagnant high-altitude air masses over Barcelona contributed to O_3 accumulation (Fig. S1.6), consistent with the ERA-INTERIM results. Notably, Fig. 5 indicates a localised transport of O_3 from Barcelona/Girona towards the Gulf of Lion.

On the early morning of 6 June (episode day in Barcelona), this contribution added to O_3 from the Gulf of Lion and returned over the Catalan coast, coinciding with the onset of the Tramontana wind (Fig. 5). This is consistent with the back trajectories analyses. At this point, there was no longer O_3 accumulation northward of the Pyrenees (circle on 6 June at 00 UTC in Fig. S1.6). On 6 June, the impact of the transported air masses from the previous day (Fig. 5) and the vertically recirculated O_3 (Fig. S1.6) in the city were observed. Simulated breezes were not intense, consistent with local observations, and this partially disrupted the Besòs-axis dynamics and facilitated the increase in O_3 in the city. Additionally, the potential impact of the weekend effect should be considered.

Simulations show vertical recirculations of O_3 towards the sea on 7 and 8 June and low O_3 levels in the Gulf of Lion. The Tramontana showed limited O_3 transport (Figs. 5 and S1.6). The O_3 accumulated aloft and over the sea surface (mostly from the preceding days) shifted southwestward, affecting other areas (Figs. 5 and S1.6). This is consistent with the observed O_3 surface concentrations, which decreased in Barcelona but still remained high in other coastal cities where the IT was exceeded,

290 e.g. Tarragona. On 8 June, a similar transport pattern was observed over the WMB with a slight decrease in the O_3 concentration, probably partially due to the restoration of weekday emissions of O_3-consuming compounds. This pattern persisted until 9 and 10 June (not shown), at which time the Tramontana wind ceased, and E winds transported surface O_3 westward, inhibiting the accumulation processes of the previous days.
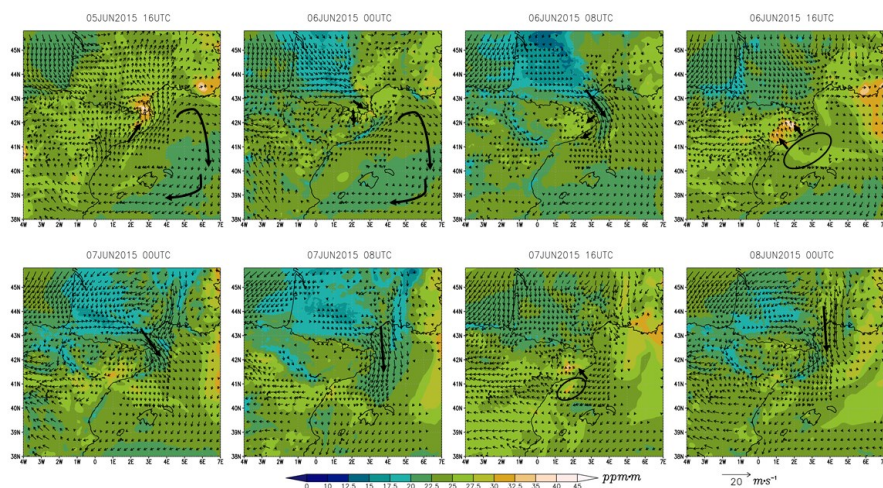
295 **Figure 5. Episode 2015. Simulated O_3 concentrations (colour scale, in ppm·m) integrated at 0–500 m above ground level (AGL) and average wind fields (vectors) between 0 and 500 m AGL. Wind speeds <2 m·s^{-1} are not represented.**

3.3 2018 Episode 2018 (4 and 5 August)

3.3.1 Meteorological context

Synoptic situation

300 From 1 to 3 August 2018, NE winds (1000–900 hPa) persisted over the W part of the European continent, from the Jutland peninsula to northern Iberia (Fig. 6), giving rise to Tramontana winds in the study area. This flow, associated with high-pressure systems over Scandinavia, extended through a broad NE–SW ridge to Iberia and North Africa. On the afternoon of 3 August, the anticyclone retreated from Jutland, strengthening W of Ireland on 4 and 5 August (episode days). Consequently, the NE winds rotated N along the Atlantic European coast, while the Tramontana persisted, driven by the pressure difference between southern France and the Mediterranean. The ERA-INTERIM reanalysis shows E winds in the Gibraltar Strait from 1

305 to 5 August, along with the Tramontana winds, following the continuity of the airflow in the marine boundary layer of the

WMB (as in Iin't Veld et al., 2021). This airflow, which was more evident at nighttime, moved into the relative lower pressure in the Gulf of Cadiz, following the eastern coast of Iberia. On 6 August, as the surface high pressures weakened in the Bay of Biscay and western France and the anticyclone shifted towards western Portugal, meteorological conditions changed, preceding the approximation of an Atlantic front through the W of the Iberian Peninsula. This marked the conclusion of the Tramontana period and the decay of the episode.
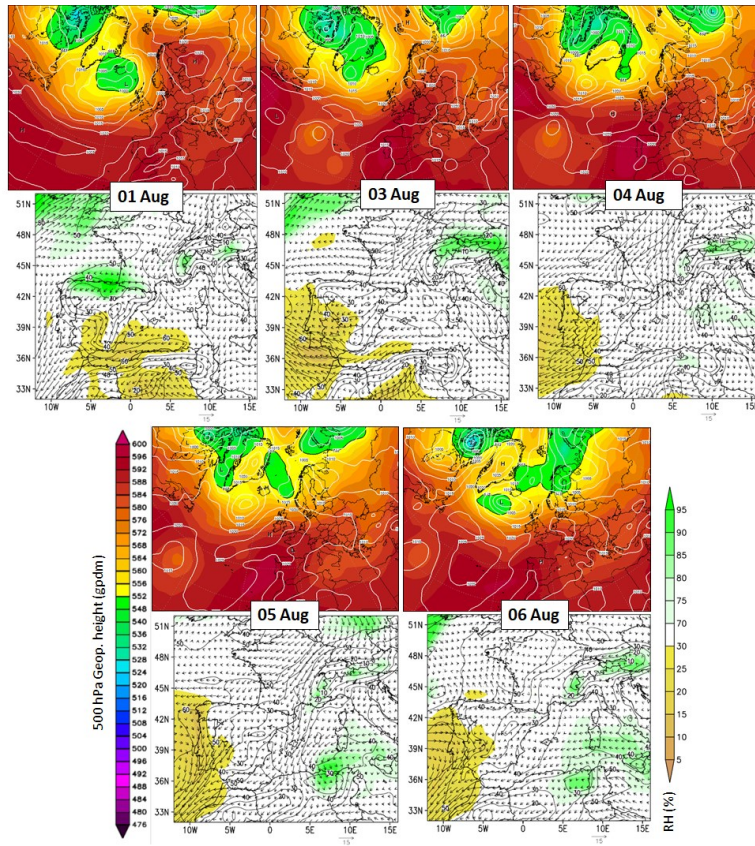
Figure 6. Episode 2018. For each day, (top) Climate Forecast System Reanalysis for the 500 hPa geopotential heights and mean sea level pressure (hPa) at 00 UTC (source: www.wetterzentrale.de), (bottom) ERA-INTERIM (ECMWF) reanalysis (0.75° resolution) of O_3 concentration (ppb, contour-lines; 1 ppb ≈ 2 µg·m^{-3} at sea level) (ppb, contour-lines), relative humidity (shaded colours) and wind field on the 950–850 hPa level.

The most intense heat episode of 2018 occurred from the first few days of August until 8 August, with coastal regions, including Barcelona, experiencing exceptionally high temperatures, and some set record highs. The peak temperatures during the episode days (Fig. S2.2b) in the city were conditioned by a light N–NE flow. This limited the tempering effect of the southerly sea breezes, which weakened during the episode, as discussed below (Meteocat, 2022).

The radiosoundings conducted in Barcelona (Fig. S2.1) show well-developed sea breezes from 1 to 3 August, also observed at the Barcelona and Parets stations (Fig. S2.2a and c). In the upper levels of the atmosphere, the wind shifted to a N pattern on 2 August at 12 UTC, which probably resulted in the entry of the upper-level polluted air masses documented by Torre-Pascual et al. (2023). On 3 and 4 August, MLHs were high between 2000 and 3000 m AGL in the city (data from 5 August are not available). The wind pattern observed at the surface on 4 and 5 August was different from the previous days, likely suggesting a weaker sea breeze development during that period (Fig. S2.2a and c), also suggested by the model simulations (see below).

3.3.2 Surface O_3 concentrations

In early August 2018, O_3 concentrations were high on a regional scale. For instance, AQMSs in S France reached extreme O_3 levels, with several AT exceedances northward from Marseille (Fig. 7a), and the Atlantic coast of the IP showed abnormally high concentrations, according to Torre-Pascual et al. (2023). Background concentrations in the study area from 1 to 3 August were high, as background stations in Barcelona (Ciutadella, Fabra and V. Hebron) recorded concentrations of up to 140 $\mu g \cdot m^{-3}$ (Fig. 7b). The Besòs-axis dynamics appear to be well established, causing very high diurnal O_3 concentrations, (up to 214 $\mu g \cdot m^{-3}$ in the Vic Plain) and multiple exceedances of the IT (Fig. 7a and c). On 3 August, peak O_3 concentrations decreased in the Vic Plain but remained close to the IT.
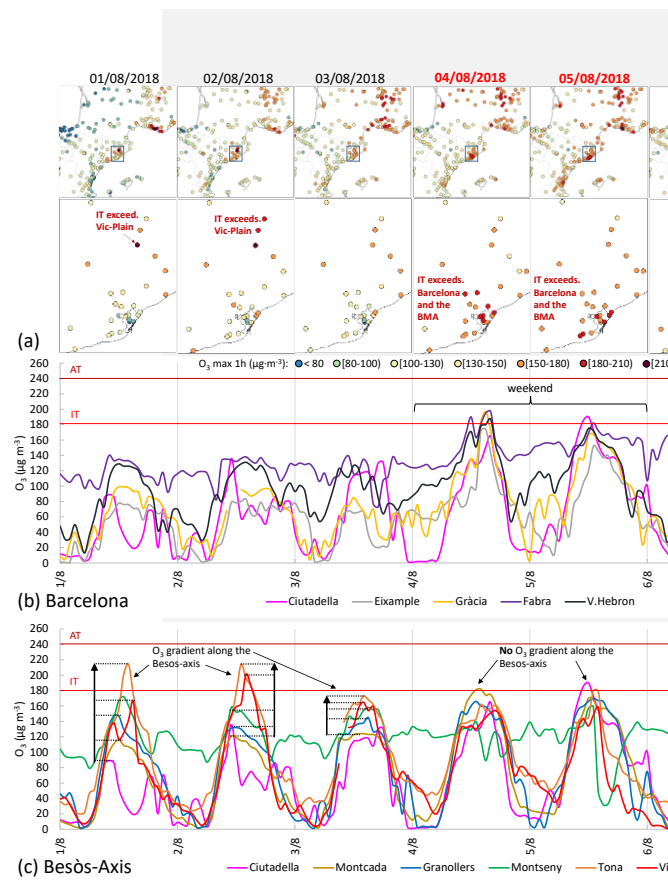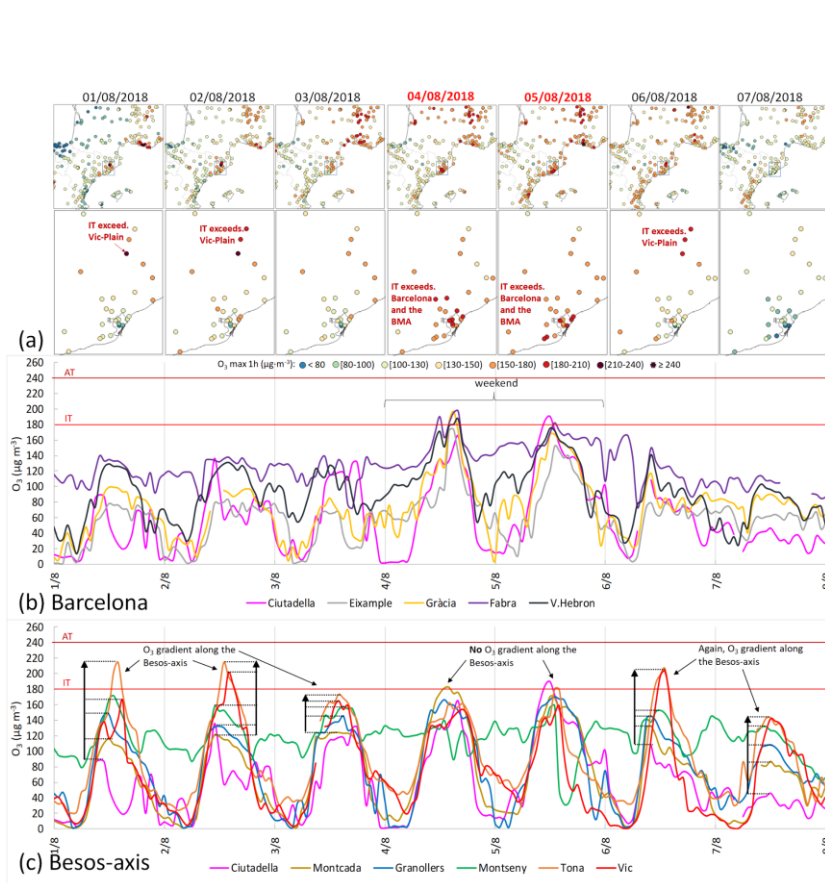
Figure 7. Episode 2018. (a) Spatial distribution of maximum hourly O₃ concentrations. Daily O₃ cycles at the surface stations: (b) Barcelona (no data from P. Reial), (c) along the Besòs-axis, ordered with increasing distance to Barcelona: Ciutadella, Montcada, Granollers, Montseny, Tona and Vic. Horizontal red lines represent the Information and Alert Thresholds of the EU's Directive (IT and AT).

During the episode in Barcelona (4 and 5 August), multiple AQMSs in the city and the BMA recorded very high O₃ concentrations, reaching up to 197 µg·m⁻³ (Fig. 7a). At the suburban Fabra station in Barcelona, exceptionally high concentrations were observed during the night of 4 to 5 August. Along the Besòs-axis, although the O₃ concentrations remained high and close to the IT, they significantly decreased compared to 1 and 2 August, and no O₃ gradient was observed (Fig. 7c), suggesting the disruption of the Besòs-axis dynamics. This resembled the 2015 episode and could have been partially attributed

to the aforementioned reduced development of breezes during the episode days and to the lower weekend precursor emissions in the BMA, as indicated by the low NOx concentrations (Fig. S2.3).

The approximation of the Atlantic front on 6 August (Monday) caused the episode in Barcelona to decay. Diurnal O_3
350 concentrations dropped to 80–140 $\mu g \cdot m^{-3}$ (Fig. 7b), especially at low-altitude stations, likely partially due to the restoration of local emissions of O_3-consuming compounds typical of workdays. The Besòs-axis dynamics seemed to re-establish, displaying a marked gradient of O_3 concentrations in AQMSs farther N and concentrations of up to 206 $\mu g \cdot m^{-3}$ in the Vic Plain (Fig. 7c).

3.3.3 Modelling output

Trajectory analyses results

355 The RAMS/HYPACT analyses (Fig. S2.4) show the arrival of tracer trajectories from central Europe to Barcelona (Fabra) on 4 and 5 August (episode days), crossing France. Air masses entered the WMB, following the Tramontana winds associated with relatively high pressures over Europe. Additionally, daytime sea breeze circulations along the E coast of Iberia generated southerly flows, potentially recirculating precursors and O_3 and adding new sources, including Tarragona and a short impact from Castellón.

360 Figure 8b shows the temporal evolution of tracer particles emitted in forward trajectories from a selection of 14 selected cities reaching the Barcelona PBL (Ciutadella). The impact of Toulouse, representing the arrival of precursors from S France, was characteristic throughout the Tramontana period. The influence from Tarragona occurred nearly every day but was not consistent. During the episode (marked with a square in Fig. 8b), a convergence of multiple sources from various regions occurred, resulting in higher overall concentrations, similar to the 2015 episode. The main sources on the episode days were
365 from central Europe, S France and the SE Iberian coast (Fig. 8c–d).
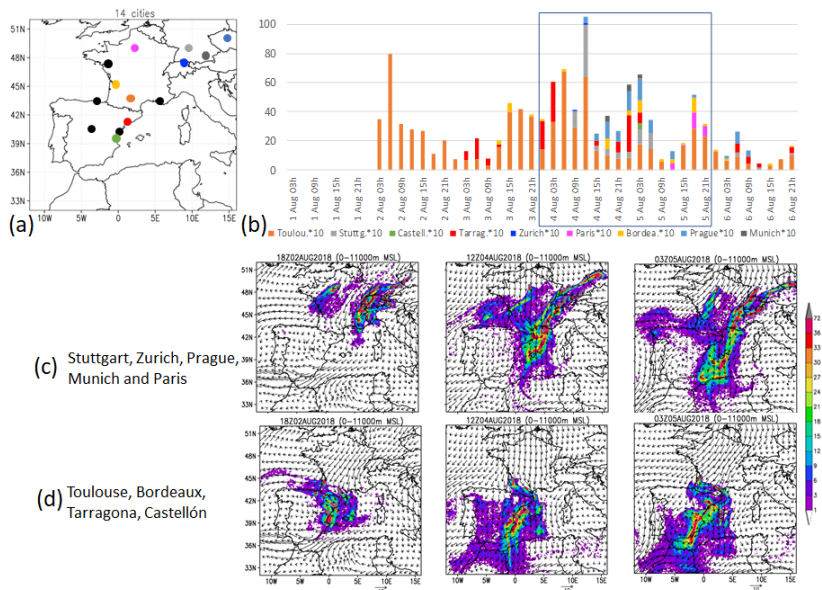
Figure 8. Episode 2018. (b) Temporal evolution of impacts (number of tracer particles) emitted from cities shown in (a) reaching Barcelona PBL (Ciutadella) in forward trajectories. Cities not represented in the bar chart had a negligible contribution, shown as black dots on the map. (c) Burden of tracer particles (0−11,000 m) impacting Barcelona emitted from Stuttgart, Zurich, Prague, Munich and Paris and (d) Toulouse, Bordeaux, Tarragona and Castellón.

Photochemical model results

The results from the photochemical simulation are shown in Figs. 9 and S2.5. The model reproduces the presence of Tramontana and accumulation of O_3 at mid-tropospheric levels across most of Iberia on 2 and 3 August (see Torre-Pascual et al., 2023). Transport of polluted air masses entering the western Mediterranean from the Gulf of Lion can be observed (Fig. 9), consistent with the trajectory results. For these days, simulations reproduced the breezes and return flows on the E coast (Figs. 9 and S2.5), causing an increase in O_3 over the sea in front of Barcelona, as also shown in the ERA-INTERIM reanalysis (Fig. 6). These mechanisms caused an accumulation of O_3 at the surface, resulting both from transport over the sea and local production.

The results indicate that on both 4 and 5 August (episode days), Barcelona was impacted by the arrival of polluted air masses from Europe through the Gulf of Lion (Figs. 9 and S2.5), consistent with the trajectory analyses. Furthermore, O_3 contributions from the S (e.g., from Tarragona) on 4 August (Fig. 9) and the accumulation of O_3 over the sea from the vertical recirculations

on the previous days affected the city. Return flows continued mixing upper-level O_3 with that situated below, contributing to more accumulation at the surface. Additionally, the intensity of the episode was likely influenced again by weakened sea breezes on 4 August (Fig. 9), as also suggested by local observations, resulting in less inland penetration of polluted air masses than on previous days. This pattern is similar to the 2015 episode. Similarly, as in the 2015 event, the weekend effect should also be considered, which likely contributed to reduced O_3 titration and ozonolysis.

On 6 August (Monday), O_3 concentrations decreased owing to meteorological changes and the recovery of O_3-consuming emissions. This decay of the episode is reflected in the simulations with the end of the Tramontana winds and the absence of discernible O_3 contributions from Europe (6 August at 00 UTC in Fig. 9).
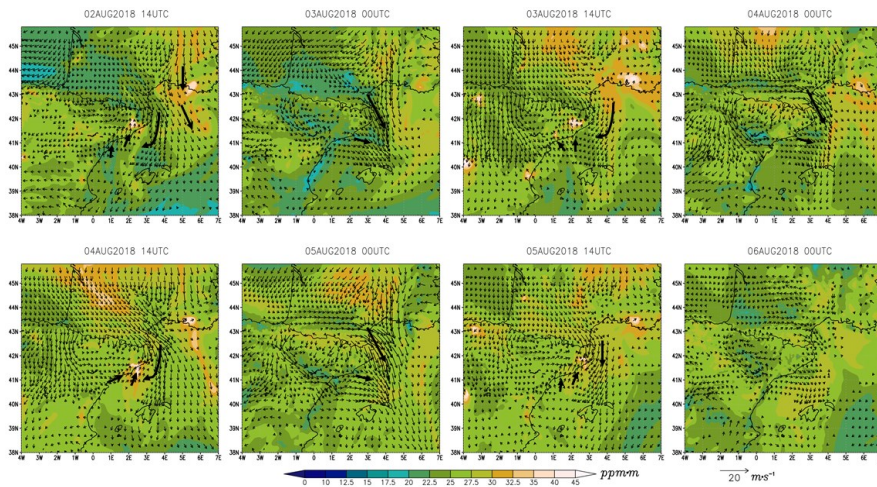
Figure 9. Episode 2018. Simulated O_3 concentrations (colour scale, in ppm·m) integrated at 0–500 m above ground level (AGL) and average wind fields (vectors) between 0 and 500 m AGL. Wind speeds <2 m·s^{-1} are not represented.

3.4 2019 episode (29 June)

3.4.1 Meteorological context

Synoptic situation

From 20 to 25 June 2019, a low-pressure centre detached from the main westerly current and moved to the NW of Iberia, weakening at the surface during its trajectory (not shown). By 25 June, it persisted as an upper-level low, isolated from the polar front. Simultaneously, a high-pressure ridge developed over the WMB after its associated African warm S winds

advanced ahead of the low-pressure centre in the Atlantic sector, inducing a heatwave event in E Iberia, including ~~in~~ Barcelona
(Fig. 10). This ridge was particularly well defined on 25 and 26 June, as mid-tropospheric S winds were observed over the
Barcelona sounding site (Fig. S3.1). In the lower layers, surface low pressures on the coasts of Portugal and the Bay of Biscay,
associated with the described upper-level low and relatively higher surface pressures on the WMB, inhibited the Tramontana
winds, suppressing the diurnal pulsation in the WMB (Gangoiti et al., 2001). This situation led to persistent easterly circulation
from the central Mediterranean to the E Iberian coast until 27 June (Fig. 10), possibly contributing to the accumulation of O_3
(55–60 ppb, ~110–120 $\mu g \cdot m^{-3}$), as also shown in the ERA-INTERIM reanalysis (see below). This was likely due to the
transport of O_3 precursors from Italy and North Africa.

On 28 June, the Atlantic low-pressure centre started displacing northwards to integrate again with a polar front trough NW of
Ireland on 30 June. During this transition, the Tramontana flow was activated, and W–NW winds prevailed up to a height of
1000–1500 m (Fig. S3.1, from 28 June at 12 UTC to 29 June), which caused a drastic decrease in humidity at surface stations
and the maximum temperature during the period, even at nighttime (see next section). The sea breeze regime and inland
convergence (SW, in Fig. S3.1) showed a very shallow (250 m) layer on 28 June at 12 UTC, influenced by a drier and warmer
Tramontana flow. These westerlies, associated with the Tramontana, continued blowing during the following day. This
situation favoured the development of return flows after the onset of the coastal easterlies and southeasterlies during the sea
breeze regime on 29 June, with subsequent pollution accumulation on the coast, as discussed in Section 3.4.3 below. Notably,
the synoptic situation during the build-up and peak of this episode was similar to the previously described 2015 episode. On
30 June, the situation changed with the onset of more intense southerlies above 1000 m in height (Fig. S3.1), preventing the
formation of sea breeze return flows and favouring venting conditions.

Local observations

The persistent easterlies before the episode were also observed at the surface with steady and relatively intense NE–E winds
(5–9 $m \cdot s^{-}$1) on 25 and 26 June (Fig. S3.2a), which combined with the southerlies above 1000 m (Fig. S3.1) likely favoured
the dispersion of pollutants to the NW. The synoptic situation described above caused Catalonia to experience an intense
heatwave from 27 to 30 June (Meteocat, 2022), peaking in maximum temperatures from 28 to 29 June. In Barcelona,
temperatures increased progressively to over 36°C on 28 June (Fig. S3.2b~d~). During the night before the episode, abnormally
high temperatures persisted, possibly due to dry westerlies observed in the soundings (29 June at 00 UTC in Fig. S3.1), with
the absolute minimum relative humidity. We interpret this as a Foehn episode of the Tramontana winds at the lee of the
mountain ranges, running parallel to the coast to the W and NW of the city. On 30 June, surface conditions shifted, with the
maximum temperatures decreasing by 5°C and the relative humidity peaking at 90%. This coincided with the onset of the
marine easterlies at lower levels (29 and 30 June) and the upper-level southerlies on 30 June (Fig. S3.1).
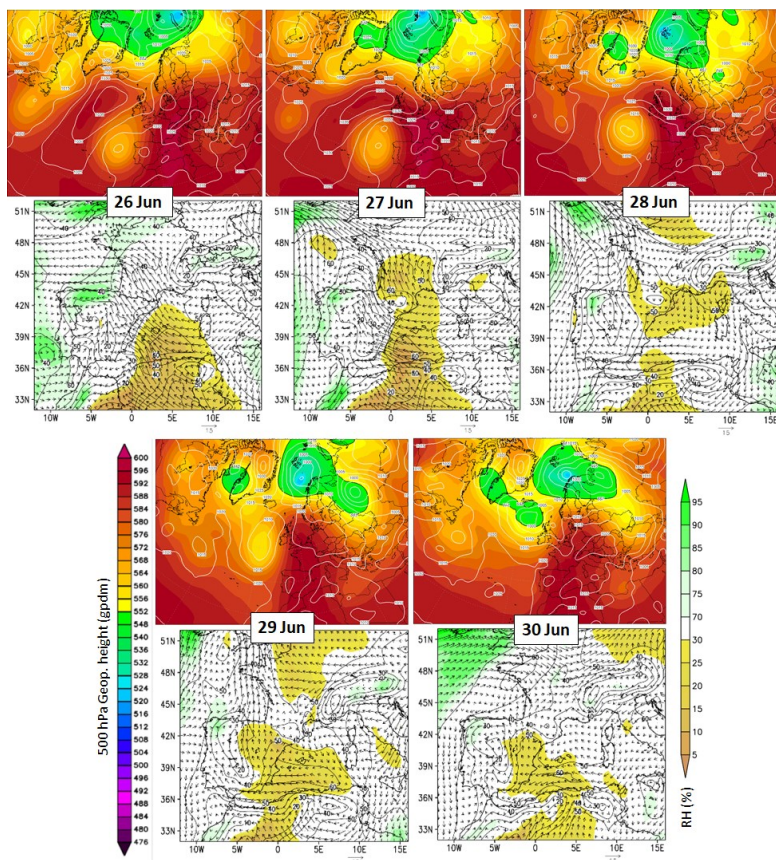
430 **Figure 10. Episode 2019. For each day, (top) Climate Forecast System Reanalysis for the 500 hPa geopotential heights and the mean sea level pressure (hPa) at 00 UTC (source: www.wetterzentrale.de), (bottom) ERA-INTERIM (ECMWF) reanalysis (0.75° resolution) of O_3 concentration (ppb, contour-lines; 1 ppb ≈ 2 µg·m^{-3} at sea level) (ppb, contour lines), relative humidity (shaded colours) and wind field at 950–850 hPa.**

3.4.2 Surface O_3 concentrations

435 On 25 and 26 June, O_3 levels in the study area were moderate for that time of year (Fig. 11a), whereas in Barcelona, concentrations (<110 µg·m^{-3}) showed little variation throughout the day (Fig. 11b). This stable pattern is attributed to the aforementioned favourable dispersion conditions, which maintained low NOx levels (Fig. S3.2), thus weakening/eliminating

nocturnal titration. On 27 June, the usual nighttime titration in Barcelona was restored (Fig. 11b), and the Besòs-axis dynamics seemed to develop (Fig. 11c), with O_3 concentrations reaching up to 193 $\mu g \cdot m^{-3}$.

440 On 28 June, O_3 concentrations increased significantly along the Besòs-axis, where the Montseny station registered extreme O_3 levels (263 $\mu g \cdot m^{-3}$). Concentrations approached the AT in the Vic Plain (Fig. 11a). Simultaneously, the AT was exceeded at stations along the NE-axis (Fig. 11a), pointing to ~~one~~ another of three possible transport routes of the BMA plume (Diéguez et al., 2009). Jaén et al. (2021), who also studied this 2019 episode, indicated that high NOx levels likely favoured O_3 production in these downwind (NOx-limited) areas. Indeed, high NO_2 levels in the morning were observed in the city, reaching

445 up to 233 $\mu g \cdot m^{-3}$ (both at the surface, as depicted in Fig. S3.3, and in the tropospheric column, as shown in Fig. S3.4). These elevated NO_2 levels could partially result from the holiday exodus, as the date coincided with a Friday preceding the vacation for a significant portion of the population. Additionally, emissions from a fire in Ribera d'Ebre (Tarragona) from 27 June onwards (clearly observed by TROPOMI, Fig. S3.4) could have contributed to the unusually high O_3 concentrations at the Montseny station (located at altitude). However, after subsequent simulations and analysis of trajectories, we concluded that

450 the fire plume passed over Barcelona at a height above 1500 m ASL on the episode day, well above the PBLH, suggesting no direct effect on O_3 levels in the city.

On Saturday, 29 June (episode in Barcelona), extreme O_3 concentrations were recorded in the city, with levels reaching up to 236 $\mu g \cdot m^{-3}$ and nearly all the active stations exceeding the IT (Fig. 11a). Interestingly, O_3 concentrations in Barcelona, especially those recorded in Fabra, exhibited a relative maximum at 10 UTC (time of low photochemical production), followed

455 by the absolute peak at approximately 15 UTC, aligning with the typical time of maximum O_3 concentrations.

In the SW BMA areas, several stations exceeded the IT, with one station exceeding the AT (Gavà, Fig. 11a). Jaén et al. (2021) attributed this pattern to a shift in the wind conditions, diverting the BMA plume (comprising recirculated and fresh emissions) westward instead of northward, which is consistent with the observed diurnal light surface winds from the E quadrant (Fig. S3.2a) and the model results (see below). Consistent with this, the O_3 daily cycles suggest an alternate BMA plume route

460 (Diéguez et al., 2009) along the Llobregat-axis instead of the Besòs-axis (Fig. 11c and d).

In the following days, the episode decayed due to the changing meteorological conditions. This is evident from the considerable decrease in O_3 concentrations, particularly at the low-altitude stations in Barcelona, with levels similar to pre-episode days (Fig. 11a).
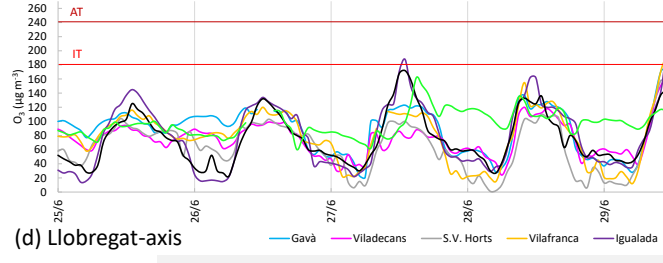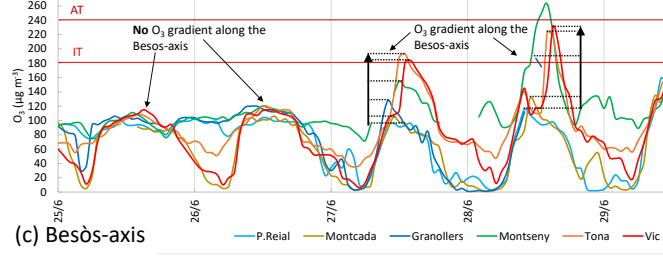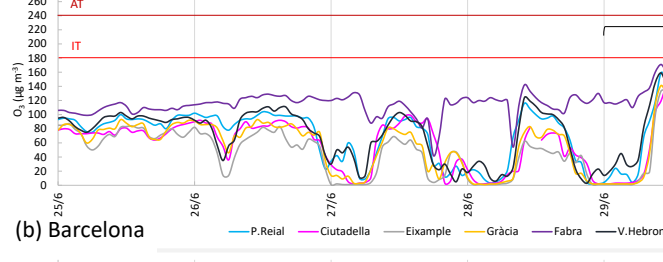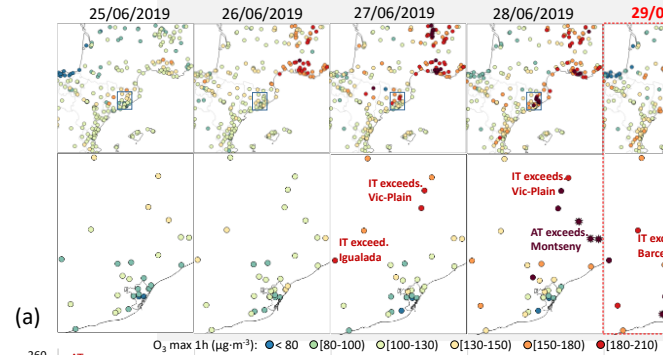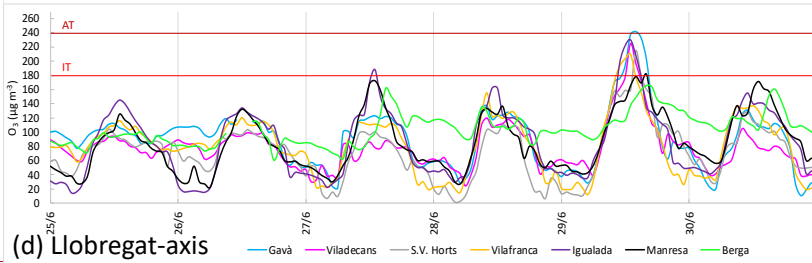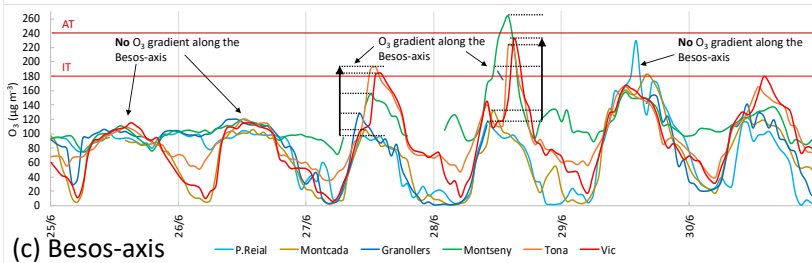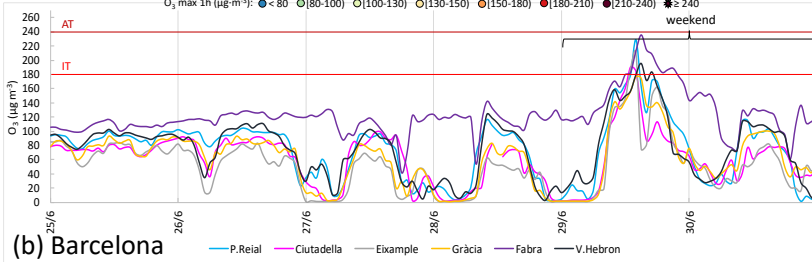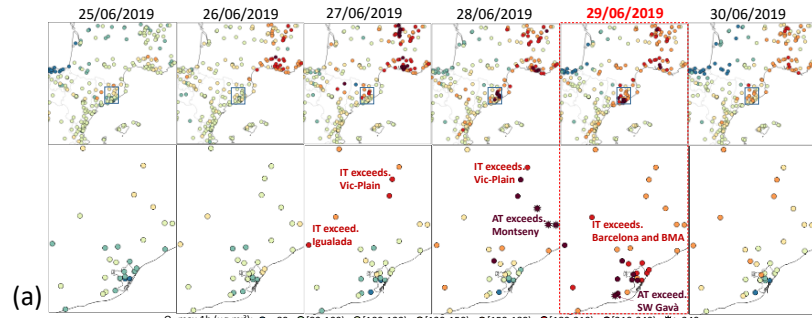
465 **Figure 11. Episode 2019. (a) Spatial distribution of maximum hourly O$_3$ concentrations. Daily O$_3$ cycles at surface stations: (b) Barcelona, (c) along the Besòs-axis, ordered with increasing distance to Barcelona: P. Reial, Montcada, Granollers, Montseny, Tona and Vic (some hourly data are missing in Granollers and Montseny) and (d) the Llobregat-axis. Horizontal red lines represent Information and Alert Thresholds of the EU's Directive (IT and AT).**

3.4.3 Modelling output

470 *Trajectory analyses results*

The RAMS/HYPACT analyses (Fig. S3.5) revealed two groups of arrival trajectories to Barcelona (Fabra) on 29 June. The first group crossed the WMB with the aforementioned easterly winds on 26 and 27 June and came from central Europe with N winds. The second group on 28 and 29 June came from the S, following the coast ("Mediterranean" contributions) with the Mediterranean Gyre circulation, and from the N with the characteristic entry through the Gulf of Lion, sweeping across S

475 France (continental European contributions).
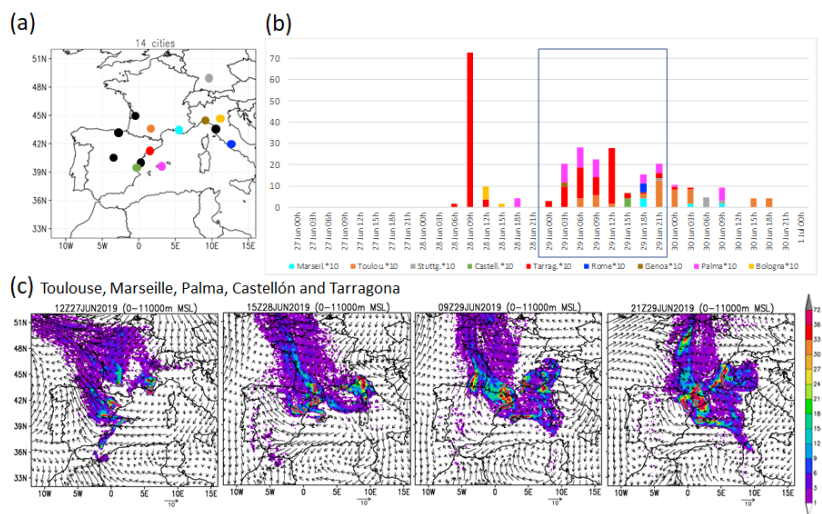
Figure 12. Episode 2019. (b) Temporal evolution of impacts (number of tracer particles) emitted from cities shown in (a) reaching Barcelona PBL (Fabra). To account for (b) variations in impact intensity between Tarragona and other cities, the concentrations of the remaining cities were multiplied by 10. Cities not represented in the (b) bar chart had negligible contributions, shown as black
480 **dots on map (a). (c) Burden of tracer particles (0−11,000 m) impacting Barcelona emitted from five selected cities: Toulouse, Marseille, Palma, Castellón and Tarragona.**

The temporal evolution of tracer particles emitted in forward trajectories from 14 selected cities (Fig. 12b) shows that the Barcelona PBL received impacts from multiple sources, as also observed in the other two episodes. The city lies in a convergence zone of N winds (Tramontana winds carrying pollution from Marseille and Toulouse) and S winds (evening anticyclonic shallow vortex with inland convergence, bringing pollutants from Tarragona, Castellón and Palma). Traces from Rome, Bologna, Genoa and Stuttgart also appeared, although to a lesser extent (with higher emissions above Barcelona). Figure 12c shows the total particle burden (0–11000 m) emitted from 5 of the 14 cities (Toulouse, Marseille, Palma, Castellón and Tarragona) before the episode (left) and during the episode (right). The joint plume initially moved westward (27 June) within the persistent easterly regime, but on 28 and 29 June, the onset of the Tramontana and the WMB circulations forced its convergence into Barcelona from the S, E and N. Thus, the results again indicate multisource convergence from the main contributors in France, Spain and Italy.

Photochemical model results

The results indicated high O_3 concentrations on 27 June along the Besòs-axis, consistent with the observed concentrations (Fig. 13). In the morning of 28 June and throughout the day, the simulated O_3 concentrations were slightly higher, shifted towards the NE and located in a relatively calmed area. This was due to the convergence of SW winds and the Tramontana wind, suggesting O_3 accumulation at the night before night. On 28 June, the sea breezes penetrated far less inland than on the previous day. The circulation induced by the Balearic daytime anticyclonic gyre carried the plume from the BMA through the Besòs-axis in a northeastward direction, coinciding with IT exceedances observed at the surface (Fig. 11a). During the night of 28 to 29 June, the Tramontana winds caused the plume to return towards the sea. This plume could be enriched with O_3 or precursors arriving from France, as inferred from the increased tropospheric NO_2 levels shown in Fig. S3.4. Simulations show high integrated O_3 concentrations over the BMA throughout that night, which with low-wind conditions, resulted in relatively high concentrations the next morning (Fig. 13).

On 29 June (episode day), off the coast of Barcelona over the sea, TROPOMI detected high levels of NO_2, consistent with the surface O_3 titration suggested by the simulations (upper panels in Fig. S3.6). This was likely caused both by a very light nocturnal sea breeze that carried precursors out to sea and by the high emissions from the holiday exodus mentioned above. During the morning and midday, with relatively weak sea breezes, the entire O_3-polluted air mass that was transported by the Tramontana during the previous day, combined with fresh NOx emissions along the coast, entered into the BMA, leading to the elevated O_3 concentrations. Notably, the surface O_3 concentrations observed in the city (Fig. 11) displayed two distinct peaks. The first peak was likely caused by fumigation of the O_3-polluted air mass before midday (bottom panels in Fig. S3.6), which was present at upper levels in a relatively warm and dry air mass and decoupled from the surface during the nighttime (Fig. S3.1). These observations highlight the presence of upper-level O_3 pollution resulting from the vertical recirculation of pollution initiated on the day before (28 June) due to the onset of the Tramontana northwesterlies and the sea breeze convergence (easterlies) at the coastal strip.

On 30 June, upper-level winds changed to S and SW, also increasing their intensity and persisting for several days (Fig. S3.1). At the surface, sea breezes penetrated further inland, with no significant return flows due to the intensity of the upper-level southerlies. The simulation reproduced this behaviour with its subsequent O_3 decrease in the BMA (not shown) and the associated decay of the episode.
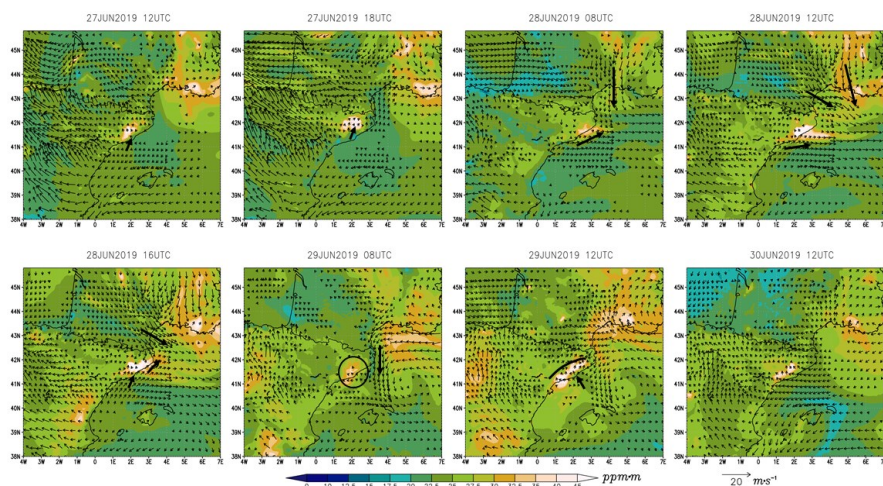
Figure 13. Episode 2019. Simulated O_3 concentrations (colour scale, in ppm·m) integrated at 0–500 m above ground level (AGL) and average wind fields (vectors) between 0 and 500 m AGL. Wind speeds <2 m·s^{-1} are not represented.

4. ~~Summary~~ Joint analysis and conclusions

Since at least the year 2000, Barcelona, situated in northeast Spain, has witnessed three extreme ozone (O_3) episodes exceeding the EU's hourly Information Threshold (180 μg·m^{-3}). These episodes, observed in the summers of 2015, 2018 and 2019, are particularly concerning, considering Barcelona's status as the second most populous city in Spain. This study aims to comprehensively analyse their phenomenology using both experimental data and modelling tools to identify key drivers and provide predictive insights.

A key finding of this study is the consistent presence of common contributing factors across the three episodes. We summarise the most significant ones, and in specific cases, provide concentration-based estimates of O_3 contributions linked to these factors, with the estimation process detailed in Section S4 (supplemental). Thus, the episodes are driven by the combined contribution of the following factors:

1. Prior O$_3$ accumulation in the coastal regions adjacent to Barcelona

This accumulation of O$_3$ results from vertical recirculation and accumulation processes in the days preceding all episodes (Querol et al., 2017 and references therein). Additionally, in the 2015 and 2019 events, a continuous contribution of O$_3$ from the Central Mediterranean is added due to a very similar synoptic situation, featuring inhibited Tramontana winds (northerly winds) and persistent easterly winds. In 2018, there is an earlier build-up of O$_3$ at mid-tropospheric levels on a regional scale (see Torre-Pascual et al., 2023). Furthermore, the higher-than-normal temperatures during all three episodes, declared as heatwaves in 2018 and 2019, might have intensified O$_3$ concentrations through various mechanisms (see Porter and Health, 2019, and references therein).

2. Weekend effect

In all cases, the episode day begins on Saturday, where the shift in pollutant emission patterns over the weekend results in an O$_3$ weekend effect, leading to an increase of approximately 15 µg·m^{-3} in O$_3$ levels. This is in a similar range as Castell-Balaguer et al.'s (2012) findings in a Mediterranean urban area within an air basin with O$_3$ phenomenology comparable to that in our study (Querol et al., 2016).

3. Presence of Tramontana during the episode

In all episodes, Tramontana meteorological conditions prevail, starting on the day of the episode (in the case of 2015) or the day before (in the episodes of 2018 and 2019). These conditions (Gangoiti et al., 2001), can lead to inhibited or weakened summer breezes and convergence over the city of polluted air masses from regional/remote sources, including the recirculation of the local metropolitan plume. In all instances, these conditions also induce the mobilisation of previously accumulated O$_3$ along the coastal areas (see Factor 1) towards the city.

4. Multiregional convergence of polluted air masses

This factor is apparent in all episodes, with O$_3$ contributions originating from at least two of the following source areas (see Section S4): (i) southern France through the Gulf of Lion (+20 µg·m^{-3}), the interior of the Mediterranean (+30−35 µg·m^{-3}), and/or eastern Spanish coastal regions (+25−30 µg·m^{-3}), including the city of Barcelona itself.

Consequently, during these extreme episodes, a contribution of at least 45−65 µg·m^{-3} is made to both the weekend effect (15 µg·m^{-3}) and the background levels, which have already initiated an accumulation in the preceding days (Factor 1).

Certain of these factors are readily observable or can be forecasted. Firstly, the observation of recirculation and accumulation processes (inferred from the analysis of daily O$_3$ cycles observed at specific monitoring stations). Secondly, the proximity to weekends or holidays, whose associated emission changes can trigger a weekend effect. Additionally, certain meteorological-

related factors can be anticipated, including heatwaves or unusually high temperatures, weakened/absent breezes, stagnation at high altitudes and/or the presence of Tramontana winds in the Western Mediterranean Basin. Considering and understanding the potential effects of these factors and their interactions to the O_3 phenomenology can contribute to the prediction of high O_3 episodes in the city.

It is important for models to accurately reproduce the processes identified in this study. A subsequent step involves quantifying the diverse contributions of O_3 and its precursors in detail, understanding their sources, and discerning key emitting sectors, among other aspects. Considering the observation that such episodes have occurred only in recent years, another future direction to explore is assessing whether urban episodes of this nature may become more prevalent in a context of global warming and declining anthropogenic emissions of O_3 precursors.

Code and data availability

The code and data utilized in this study are accessible upon request via email (jordi.massague@idaea.csic.es).

Since at least the year 2000, Barcelona has experienced three extreme ozone (O_3) episodes in which the EU's hourly Information Threshold (180 μg·m^{-3}) was exceeded. These episodes occurring in the summers of 2015, 2018 and 2019 were concerning, especially considering that Barcelona is the second most populous city in Spain. This study aimed to analyse their phenomenology comprehensively through experimental data and modelling tools to identify drivers and common patterns, and offer predictive insights.

JM: Conceptualization; Data curation; Formal analysis; Investigation; Methodology; Software; Validation; Visualization; Writing – original draft; Writing – review & editing

ET-P: Conceptualization; Data curation; Formal analysis; Investigation; Methodology; Software; Validation; Visualization; Writing – original draft; Writing – review & editing

CC: Conceptualization; Data curation; Formal analysis; Investigation; Methodology; Software; Visualization; Writing – review & editing

ME: Conceptualization; Formal analysis; Investigation; Supervision; Methodology; Software; Validation; Visualization; Writing – original draft; Writing – review & editing

AA: Investigation; Funding acquisition; Supervision; Formal analysis; Investigation; Methodology; Software; Validation; Visualization; Writing – original draft; Writing – review & editing

MP: Data curation; Formal analysis; Investigation; Methodology; Software; Visualization; Writing – review & editing

XQ: Conceptualization; Formal analysis; Funding acquisition; Investigation; Supervision; Methodology; Validation; Visualization; Writing – original draft; Writing – review & editing

GG: Conceptualization; Data curation; Formal analysis; Investigation; Supervision; Methodology; Software; Validation; Visualization; Writing – original draft; Writing – review & editing

590 **Competing interests**

At least one of the (co-)authors is a member of the editorial board of Atmospheric Chemistry and Physics

Acknowledgements

This study is supported by the Spanish Ministry of Ecological Transition and Demographic Challenge, in the framework of the Spanish Ozone Abatement Plan. The IDAEA-CSIC team also acknowledges the support received from the Generalitat de
595 Catalunya (AGAUR 2021 SGR 00447). The UPV/EHU team acknowledges the University of the Basque Country UPV/EHU as the source of the financial support: GIA consolidated Research Groups (GIU21/050) (https://www.ehu.eus/es/web/gia), and the Spanish Ministry of Universities and the European Union, for the Margarita Salas Grant (MARSA21/23) of Eduardo Torre-Pascual, funded by the European Union-Next Generation EU. These financing bodies have played an exclusively economic role in the study. We would also like to thank express our gratitude to Yolanda Sola (University of Barcelona, Faculty of
600 Physics) for providing data from the radiosoundings, Ana Rodríguez-García for producing figures for the validation of the photochemical model simulations, EEA for the air quality data from European monitoring stations, Meteocat for the meteorological surface data, the ESA for remote-sensing NO_2 data (Sentinel-5 Precursor, TROPOMI), Wetterzentrale.de for the synoptic maps and QGIS for their open-source GIS software. Finally, we want to acknowledge the anonymous reviewers whose insightful comments and discussions significantly contributed to improve this work.

605 ## 65. References

Barros, N., Borrego, C., Toll, I., Soriano, C., Jiménez, P., and Baldasano, J. M.: Urban Photochemical Pollution in the Iberian Peninsula: Lisbon and Barcelona Airsheds, J. Air Waste Manage. 53, 347–359, 2003.

Castell, N., Mantilla, E., and Millán, M. M.: Analysis of tropospheric ozone concentration on a Western Mediterranean site: Castellon (Spain), Environ. Monit. Assess., 136, 3–11, 2008.

610 Batista e Silva F., Dijkstra L., Poelman H.: The JRC-GEOSTAT 2018 population grid. JRC Technical Report. Forthcoming, 2021.

Chevalier, A., Gheusi, F., Delmas, R., Ordonez, C., Sarrat, C., Zbinden, R., Thouret, V.,Athier, G., Cousin, J.M. : Influence of altitude on ozone levels and variability in the lower troposphere: a ground-based study for western Europe over the period 2001–2004. Atmos. Chem. Phys. 7, 4311–4326, 2007.

615 Crippa, M., Guizzardi, D., Muntean, M., Schaaf, E., Dentener, F., van Aardenne, J. A., Monni, S., Doering, U., Olivier, J. G. J., Pagliari, V., and Janssens-Maenhout, G.: Gridded emissions of air pollutants for the period 1970–2012 within EDGAR v4.3.2, Earth System Science Data, 10(4), 1987-2013, https://doi.org/10.5194/essd-10-1987-2018, 2018.

Dieguez, J. J., Millán, M., Padilla, L., and Palau, J. L.: Estudio y evaluación de la contaminación atmosférica por ozono troposférico en España, CEAM Report for the Ministry of Agriculture, Food and Environment, INF FIN/O3/2009, 372 pp.,

620 2009.

Dieguez, J. J., Calatayud, V., and Mantilla, E.: CEAM Report for the Ministry of Agriculture, Food and Environment, Fundación Biodiversidad, Informe Final, Memoria Técnica Proyecto CONOZE, CONtaminación por OZono en España, 137 pp., 2014.

EEA: Air quality in Europe – 2015 report, EEA Report, No 5/2015, ISSN 1977-8449, 57 pp., 2015.

625 EEA: Air quality in Europe–2020 report, European Environment Agency. EEA Report, No 09/2020 (ISSN 1977-8449), 160 pp. doi: 10.2800/786656, 2020.

EC. Directive 2008/50/EC, Of The European Parliament And Of The Council of 21 May 2008 on ambient air quality and cleaner air for Europe http://eur-lex.europa.eu/legal-content/ES/TXT/?uri=CELEX:32008L0050, last access: 30 December 2022, 2008.

630 EPA: U.S. Environmental Protection Agency. SPECIATE Version 4.5. Database Development Documentation. EPA/600/R-16/294, https://www.epa.gov/sites/default/files/2016-09/documents/speciate_4.5.pdf, 2016.

Escudero, M., Segers, A., Kranenburg, R., Querol, X., Alastuey, A., Borge, R., de la Paz, D., Gangoiti, G., and Schaap, M.: Analysis of summer O3 in the Madrid air basin with the LOTOS-EUROS chemical transport model, Atmos. Chem. Phys., 19, 14211–14232, https://doi.org/10.5194/acp-19-14211-2019, 2019.

635 Fowler, D., Pilegaard, K., Sutton, M. A., Ambus, P., Raivonen, M., et al.: Atmospheric composition change: Ecosystems-Atmosphere interactions, Atmos. Environ., 43, 5193–5267, https://doi.org/10.1016/j.atmosenv.2009.07.068, 2009.

Gangoiti, G., Millán, M. M., Salvador, R., and Mantilla, E.: Long range transport and re-circulation of pollutants in the western Mediterranean during the project Regional Cycles of Air Pollution in the West-Central Mediterranean Area, Atmos. Environ., 35, 6267–6276, 2001.

640 Gangoiti, G. Alonso, L., Navazo, M., Albizuri, A.Perez-Landa, G., Matabuena, M., Valdenebro, V. et al.: Regional transport of pollutants over the Bay of Biscay: analysis of an ozone episode under a blocking anticyclone in west-central Europe Atmos. Environ., 36, 8, pp. 1349-1361, 10.1016/S1352-2310(01)00536-2, 2002.

Gangoiti, G., Albizuri, A., Alonso, L., Navazo, M., Matabuena, M., et al: Sub-continental transport mechanisms and pathways during two ozone episodes in northern Spain. Atmos. Chem. Phys., 6, pp. 1469-1484., 2006.

645 Gangoiti, G., Sáez de Cámara, E., Alonso, L., Navazo, Gómez, M.C., Iza, J., García, J. A., Ilardia, J. L., and Millán M.M.: Origin of the water vapor responsible for the European extreme rainfalls of August 2002: 1. High-resolution simulations and tracking of air masses. J. Geophys. Res., 2011.

GBD: Global Burden of Disease Study 2016 Cause-Specific Mortality 1980–2016, Seattle, United States: Institute for Health Metrics and Evaluation (IHME), 2016.

650 Gencat: Llista de superacions i informes anuals. Medi Ambient i Sostenibilitat., 2022. https://mediambient.gencat.cat/ca/05_ambits_dactuacio/atmosfera/qualitat_de_laire/avaluacio/campanya_ozo/Llista-superacions-i-informes-anuals/, Last accessed on 2022-07-14, 2022.

Gorelick, N., Hancher, M., Dixon, M., Ilyushchenko, S., Thau, D., Moore, R.,: Google Earth Engine: planetary-scale geospatial analysis for everyone. Remote Sens. Environ. 202, 18–27., 2017.

655 Guo, Y., Gasparrini, A., Armstrong, B. G., Tawatsupa, B., Tobias, A., et al.: Temperature variability and mortality: a multi-country study, Environ. Health Persp., 124, 1554–1559, 2017.

Heuss, J.M., Kahlbaum, D.F., Wolff, G.T.: Weekday/Weekend ozone differences: what can we learn from them? J. Air Waste Manag. Assoc., 53, pp. 772-788, 2003.

Holzworth, G. C.: Estimates of mean maximum mixing depths in the contiguous United States, Mon. Weather Rev., 92, 235–
660 242, 1964.

In't Veld, M., Carnerero, C., Massagué, J., Alastuey, A., de la Rosa, J., et al: Understanding the local and remote source contributions to ambient O3 during a pollution episode using a combination of experimental approaches in the Guadalquivir valley, Southern Spain. Science of The Total Environment. 777. 144579. https://doi.org/10.1016/j.scitotenv.2020.144579, 2021.

665 IPCC: Climate Change 2021: The Physical Science Basis. Contribution of Working Group I to the Sixth Assessment Report of the Intergovernmental Panel on Climate Change. Cambridge University Press, Cambridge, United Kingdom and New York, NY, USA, 2391 pp., doi:10.1017/9781009157896, 2021.

Jaén, C. Udina, M., Bech, J.: Analysis of two heat wave driven ozone episodes in Barcelona and surrounding region: Meteorological and photochemical modeling. Atmospheric Environment., 146, 118037.
670 https://doi.org/10.1016/j.atmosenv.2020.118037, 2021.

Jiménez, P., Parra, R., Gassó, S., Baldasano, J.M.: Modeling the ozone weekend effect in very complex terrains: a case study in the Northeastern Iberian Peninsula. Atmos. Env., 39, 3, 429-444. https://doi.org/10.1016/j.atmosenv.2004.09.065, 2005.

Kalabokas, P., Hjorth, J., Foret, G., Dufour, G., Eremenko, M., Siour, G., Cuesta, J., and Beekmann, M.: An investigation on the origin of regional springtime ozone episodes in the western Mediterranean, Atmos. Chem. Phys., 17, 3905–3928,
675 https://doi.org/10.5194/acp-17-3905-2017, 2017.

Langner, J., Engardt, M., Baklanov, A., Christensen, J. H., Gauss, M., Geels, C., Hedegaard, G. B., Nuterman, R., Simpson, D., Soares, J., Sofiev, M., Wind, P., and Zakey, A.: A multi-model study of impacts of climate change on surface ozone in Europe, Atmos. Chem. Phys., 12, 10423–10440, doi:10.5194/acp-12-10423-2012, 2012.

Massagué, J., Carnerero, C., Escudero, M., Baldasano, J. M., Alastuey, A., and Querol, X.: 2005–2017 ozone trends and
680 potential benefits of local measures as deduced from air quality measurements in the north of the Barcelona metropolitan area, Atmos. Chem. Phys., 19, 7445–7465, https://doi.org/10.5194/acp-19-7445-2019, 2019.

Massagué, J., Escudero, M., Alastuey, A., Mantilla, E., Monfort, E., Gangoiti, G., Pérez García-Pando, C., and Querol, X.: Spatiotemporal variations of tropospheric ozone in Spain (2008–2019). Env. Int., 176, 107961, ttps://doi.org/10.1016/j.envint.2023.107961, 2023.

685 Meteocat: Butlletí climàtic mensual. Servei Meteorològic de Catalunya https://www.meteo.cat/wpweb/climatologia/el-clima-ara/butlleti-mensual/, Last accessed on 2022-06-01., 2022.

MITMA: Áreas Urbanas en España, 2021. Ministerio de Transportes, Movilidad y Agencia Urbana, DG de Vivienda y Suelo. NIPO: 796-20-112-X. https://www.mitma.gob.es/portal-del-suelo-y-politicas-urbanas/atlas-estadistico-de-las-areas-urbanas, Last accesses: 2022-10-10, 2021.

690 Millán M.M., Salvador R., Mantilla E., and Kallos G.: Photooxidant dynamics in the Mediterranean basin in summer: Results from European research projects, Journal of Geophysical Research 102, 8811-8823, 1997.

Millán M.M., Mantilla E., Salvador R., Carratalá A., Sanz M.J., Alonso L., Gangoiti G., and Navazo M.: Ozone Cycles in the Western Mediterranean Basin: Interpretation of Monitoring Data in Complex Coastal Terrain, Journal of Applied Meteorology, 39: 487-508, 2000.

695 Millán, M. M., Sanz, M. J., Salvador, R., and Mantilla, E.: Atmospheric dynamics and ozone cycles related to nitrogen deposition in the western Mediterranean, Environ. Pollut., 118, 167–186, 2002

Millán, M. M.: Extreme hydrometeorological events and climate change predictions in Europe, J. Hydrol., 518B, 206–224, 2014.

Monks P.S., Archibald A.T., Colette A., Cooper O., Coyle M., et al.: Tropospheric ozone and its precursors from the urban to
700 the global scale from air quality to short-lived climate forcer, Atmospheric Chemistry and Physics, 15, 8889-8973, 2015.

Observatori Fabra: Secció Meteorològica. http://www.fabra.cat/meteo/resums/resums2015.html. Last accessed on 2022-08-01., 2022.

Pay, M. T., Gangoiti, G., Guevara, M., Napelenok, S., Querol, X., Jorba, O., and Pérez García-Pando, C.: Ozone source apportionment during peak summer events over southwestern Europe, Atmos. Chem. Phys., 19, 5467–5494,
705 https://doi.org/10.5194/acp-19-5467-2019, 2019.

Pérez C. et al.: Summertime re-circulations of air pollutants over the north-eastern Iberian coast observed from systematic EARLINET lidar measurements in Barcelona. Atmospheric Environment 38 (2004) 3983–4000, 2004.

Porter, W. C. and Heald, C. L.: The mechanisms and meteorological drivers of the summertime ozone–temperature relationship, Atmos. Chem. Phys., 19, 13367–13381, https://doi.org/10.5194/acp-19-13367-2019, 2019.

710 Pu X., Wang T., Huang X., Melas D., Zanis P., Papanastasiou D., Poupkou A. Enhanced surface ozone during the heat wave of 2013 in yangtze river Delta region, China Sci. Total Environ., 603, pp. 807-816., 2017.

Querol X., Alastuey A., Orio A., Pallares M., Reina F., Dieguez J. J., Mantilla E., Escudero M., Alonso L., Gangoiti G., Millán M.: On the origin of the highest ozone episodes in Spain, Science of the Total Environment, 572, 379-389, 2016.

Querol X., Gangoiti G., Mantilla E., Alastuey A., Minguillón M. C., et al.: Phenomenology of high-ozone episodes in NE
715 Spain, Atmospheric Chemistry and Physics, 17, 2817-2838, 2017.

Ramboll Environment and Health: User's Guide: Comprehensive Air Quality Model with Extensions. Version 6.5, Novato, California, https://camx-wp.azurewebsites.net/Files/CAMxUsersGuide_v6.50.pdf, 2018.

Seco, R., Peñuelas, J., Filella, I., Llusià, J., Molowny-Horas, R., Schallhart, S., Metzger, A., Müller, M., and Hansel, A.: Contrasting winter and summer VOC mixing ratios at a forest site in the Western Mediterranean Basin: the effect of local biogenic emissions, Atmos. Chem. Phys., 11, 13161–13179, https://doi.org/10.5194/acp-11-13161-2011, 2011.

Sillman, S.: The relation between ozone, NOx and hydrocarbons in urban and polluted rural environments. Atmos Environ 33: 1821–1845. DOI: https:// doi.org/10.1016/S1352-2310(98)00345-8, 1999.

Sillman, S., and He, D.: Some theoretical results concerning O3-NOx-VOC chemistry and NOx-VOC indicators, J. Geophys.Res.,107(D22), 4659, doi:10.1029/2001JD001123, 2002.

Solberg, S., Bergström, R., Langner, J., Laurila, T., Lindskog, A.: Changes in Nordic surface ozone episodes due to European emission reductions in the1990s. Atmos. Environ. 39, 179–192, 2005

Toll, I. and Baldasano, J. M.: Modeling of photochemical air pollution in the Barcelona area with highly disaggregated anthropogenic and biogenic emissions, Atmos. Environ., 34, 3069–3084, https://doi.org/10.1016/S1352-2310(99)00498-7, 2000.

Torre-Pascual, E., Sáez de Cámara, E., Gangoiti, G., and Zuazo, I.: Biogenic VOC Emission Modeling for Spain: Adaptation of the National Forest Inventory as Input for MEGANv3, Air Pollution Modeling and its Application XXVII, Mensink, C., Volker, M. (Eds.), 45-50, Springer, https://doi.org/10.1007/978-3-662-63760-9_7, 2021.

Torre-Pascual, E., Gangoiti, G., Rodríguez-García, A., Sáez de Cámara, E., Ferreira, J., Gama, C., Gómez, M. C., Zuazo, I., García, J. A., and de Blas, M.: Analysis of an intense O_3 pollution episode in the Atlantic Coast of the Iberian Peninsula using photochemical modelling: characterization of transport pathways and accumulation processes, EGUsphere [preprint], https://doi.org/10.5194/egusphere-2023-387, 2023.

Valverde, V., Pay, M.T., Baldasano, J.M.: Ozone attributed to Madrid and Barcelona on-road transport emissions: characterization of plume dynamics over the Iberian Peninsula. Sci. Total Environ. 543, 670–682., 2016.

Van Geffen, J., Eskes, H.J., Boersma, K.F., Maasakkers, J.D., Veefkind, J.P.: TROPOMI ATBD of the total and tropospheric NO2 data products. Royal Netherlands Meteorological Institute, #S5P-KNMI-L2–0005-RP, Issue 1.4.0, 2019.

Vautard, R., Beekmann, M., Desplat, J., Hodzic, A., and Morel, S.: Air quality in Europe during the summer of 2003 as a prototype of air quality in a warmer climate, CR Geosci., 339, 747–763, https://doi.org/10.1016/j.crte.2007.08.003, 2007.

Veefkind, J.P., Aben, I., McMullan, K., Föorster, H., deVries, J., Otter, G., Claas, J., Eskes, H.J., De Haan, J.F., Kleipool, Q., Van Weele, M.: TROPOMI on the ESA Sentinel-5 Precursor: a GMES mission for global observations of the atmospheric composition for climate, air quality and ozone layer applications. Remote Sens. Environ. 120, 70–83. https://doi.org/10.1016/j.rse.2011.09.027., 2012.

WHO: Air Quality Guidelines: Global Update 2005, Particulate matter, ozone, nitrogen dioxide and sulfur dioxide, World Health Organisation, Copenhagen, 484 pp., available at: http://www.euro.who.int/__data/assets/pdf_file/0005/78638/E90038.pdf (last access: 23 November 2017), 2006.

750   WHO Regional Office for Europe: Health Risks of Air Pollution in Europe–HRAPIE Project: Recommendations for Concentration-Response Functions for Cost–Benefit Analysis of Particulate Matter, Ozone and Nitrogen Dioxide, Copenhagen, 65 pp., available at: http://www.euro.who.int/__data/assets/pdf_file/0017/234026/e96933.pdf?ua=1 (last access: 5 April 2022), 2013b.

WHO: Global Air Quality Guidelines. Particulate matter (PM2.5 and PM10), ozone, nitrogen dioxide, sulphur dioxide and
755   carbon monoxide. Geneva: World Health Organization, available at: https://www.who.int/publications/i/item/9789240034228 (last access: 25 January 2021), 2021.